Synthesis, Cannabinoid Receptor Affinity, and Molecular Modeling Studies of Substituted 1-Aryl-5-(1*H*-pyrrol-1-yl)-1*H*-pyrazole-3-carboxamides

Romano Silvestri,*[,†] Maria Grazia Cascio,[⊥] Giuseppe La Regina,[†] Francesco Piscitelli,[†] Antonio Lavecchia,*[,§] Antonella Brizzi,[‡] Serena Pasquini,[‡] Maurizio Botta,[‡] Ettore Novellino,[§] Vincenzo Di Marzo,[⊥] and Federico Corelli*[,‡]

Istituto Pasteur—Fondazione Cenci Bolognetti, Dipartimento di Studi Farmaceutici, Sapienza Università di Roma, Piazzale Aldo Moro 5, I-00185 Roma, Italy, Dipartimento Farmaco Chimico Tecnologico, Università di Siena, Polo Scientifico Universitario San Miniato, Via Aldo Moro 2, I-53100 Siena, Italy, Dipartimento di Chimica Farmaceutica e Tossicologica, Università di Napoli Federico II, Via Domenico Montesano 49, I-80131, Napoli, Italy, and Istituto di Chimica Biomolecolare, Consiglio Nazionale delle Ricerche, Via Campi Flegrei 34, Comprensorio Olivetti, I-80078 Pozzuoli, Napoli, Italy

Received May 15, 2007

The new 1-phenyl-5-(1*H*-pyrrol-1-yl)pyrazole-3-carboxamides were compared with the reference compounds AM251 and SR144528 for cannabinoid hCB_1 and hCB_2 receptor affinity. Compounds bearing 2,4-dichlorophenyl or 2,4-difluorophenyl groups at position 1 and 2,5-dimethylpyrrole moiety at position 5 of the pyrazole nucleus were generally more selective for hCB_1. On the other hand, the *N*-cyclohexyl group at the 3-carboxamide was the determinant for the hCB_2 selectivity, in particular when a 3,4-dichlorophenyl group was also present at position 1. Compound **26** was the most selective ligand for the hCB_1 receptor (K_i (CB_2)/K_i (CB_1) = 140.7). Derivative **30**, the most potent hCB_1 ligand (K_i = 5.6 nM), was equipotent to AM251 and behaved as an inverse agonist in the cAMP assay (EC_{50} ~1 nM). The carbonyl oxygen of both **26** and **30** formed a H-bond with K3.28(192), while the substituents at the nitrogen fitted in a pocket formed by lipophilic residues. This H-bonding interaction was proposed to account for the high affinity for receptors' inactive state and the inverse agonist activity.

Introduction

The endocannabinoid system is formed by three key components, the CB_1[a] and CB_2 cannabinoid receptors, their endogenous ligands (endocannabinoids), and enzymes, proteins, and transporters involved in endocannabinoid formation and inactivation.[1,2] The endocannabinoid system is correlated to an ever increasing number of pathological conditions (pain, immunosuppression, peripheral vascular disease, appetite enhancement or suppression, and locomotor disorders), which show excellent targets for the development of new drugs.[3–5]

The neuromodulatory action of endocannabinoids through CB_1 receptors regulates locomotor activity, learning, memory, emotion, motivation, and appetite.[1,6] Targeting cannabinoid receptors may be a useful way to treat motor disorders, such as Parkinson's disease,[7] Tourette's syndrome,[8] or choreas,[9] with further therapeutic applications in controlling airway responsiveness,[10] intraocular pressure,[11] and intestinal motility.[12] Currently, CB_1 receptor antagonists and inverse agonists[13] are evaluated for obesity, metabolic disorders, smoking cessation, and alcohol abuse.[13,14] On the other hand, selective CB_2 ligands may be used to treat pain,[15] inflammation,[16] osteoporosis,[17] CB_2-receptor-expressing malignant gliomas,[18] tumors of immune origin,[19] and immunological disorders such as multiple sclerosis.[20]

Rimonabant (SR141716, **1**) is a potent and selective antagonist for the CB_1 receptor. It was launched in 2006 by Sanofi-Aventis for the treatment of obesity and associated risk factors.[13,21,22] In clinical trials, **1** showed CNS (depression anxiety, dizziness, and insomnia) and gastrointestinal (nausea, diarrhea) side effects.[23] Several pyrazole analogues[24] of **1** have been synthesized: 1,5-diarylpyrazoles (AM251[25] (**2**) and SR147778[21a] (**3**)), 1,4-diarylpyrazoles (AM281[26] (**4**)), and 3,4-diarylpyrazoles (SLV319[27] (**5**) and SLV326[27] (**6**)). On the other hand, simple chemical modification of the 1,5-diarylpyrazole scaffold led to selective CB_2 ligands, for example SR144528[28] (**7**; Chart 1).

New cannabinoid receptor–ligands were discovered by replacing the central pyrazole nucleus with bioisosteric heterocycles. For example, 4,5-diarylimidazoles[29] (**8**), 1,2-diarylimidazoles[30] (**9**), and 1,5-diarylpyrroles[31] (**10**) closely related to **1** showed to be potentially useful to treat obesity. CB_1 antagonists were also obtained by expanding the pyrazole core to 6-membered rings, such as benzene,[32] pyridine,[33] or pyrimidine.[34]

We decided to pursue a bioisosteric approach entailing not the replacement of the central pyrazole nucleus, but the substitution of a pyrrole ring for the 4-chlorophenyl group at position 5 of **1**. Based on our know-how in pyrrole bioisosterism,[35] this modification was expected to provide highly potent ligands.

In this paper we describe the synthesis and hCB_1 and hCB_2 receptor affinity of potent pyrrole bioisosteres **11**–**19** and **22**–**44**, characterized by different substitutions at the 1-phenyl ring and at the 3-carboxamide nitrogen (Table 1). For comparison purposes, the two isomeric 4-carboxamides **20** and **21**, structurally related to pyrazole derivatives previously reported by us,[36]

* To whom correspondence should be addressed. Phone: +39 06 4991 3800 (R.S.); +39 081 678 613 (A.L., molecular modeling); +39 0577 234308 (F.C.). Fax: +39 06 491 491 (R.S.); +39 081 678 613 (A.L.); +39 0577234299(F.C.).E-mail:romano.silvestri@uniroma1.it(R.S.);lavecchi@unina.it (A.L.); corelli@unisi.it (F.C.).

† Università di Roma.

‡ Università di Siena.

§ Università di Napoli Federico II.

⊥ Consiglio Nazionale delle Ricerche di Pozzuoli.

[a] Abbreviations: CB, cannabinoid; TM, transmembrane; SAR, structure–activity relationship; MD, molecular dynamics; GPCR, G protein-coupled receptor; EL, extracellular loop; WT, wild type; S.I., selectivity index; EDC, *N*-(3-dimethylaminopropyl)-*N*′-ethylcarbodiimide hydrochloride; HOBt, 1-hydroxybenzotriazole.

10.1021/jm070566z CCC: $40.75
Published on Web 02/23/2008

Chart 1. Selective CB_1 and CB_2 Ligands

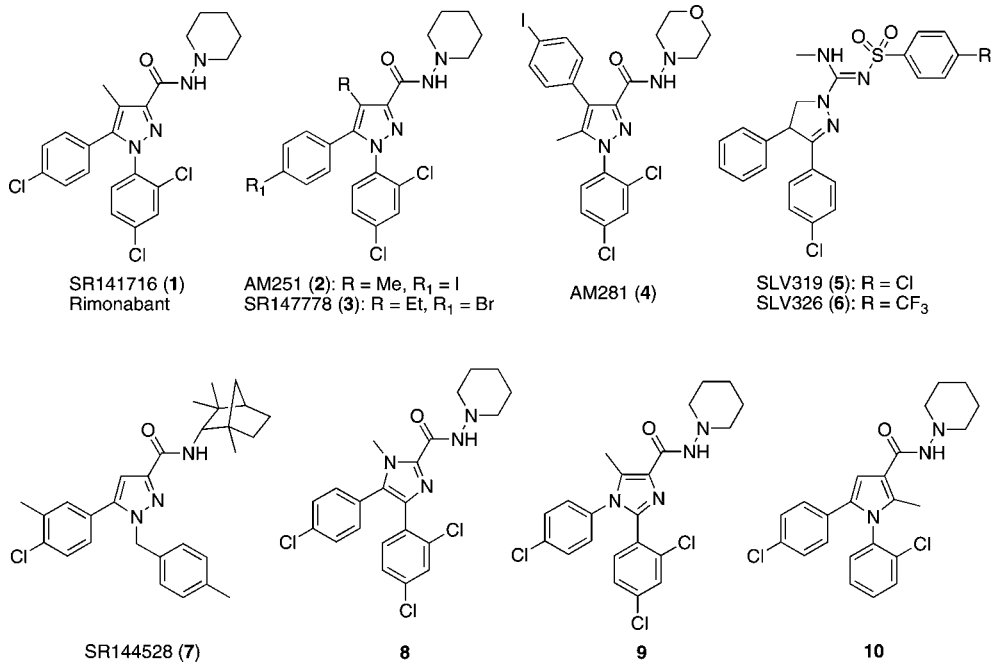

were also synthesized. To rationalize the binding results, we depicted the putative transmembrane (TM) binding motif on the hCB_1 receptor by molecular modeling. Structure–activity relationships (SARs) were explained by analyzing the three-dimensional (3-D) structure of the inverse agonist/receptor models obtained by molecular docking and molecular dynamics (MD) simulations.

Chemistry. Potassium 1-cyano-3-ethoxy-3-oxoprop-1-en-2-olate (**45**) was obtained by treatment of diethyl oxalate with acetonitrile in the presence of 18-crown-6 and potassium *tert*-butoxide (Scheme 1). Reaction of **45** with phenylhydrazine and 37% HCl or 4-chlorophenylhydrazine hydrochloride in refluxing ethanol furnished ethyl 1-phenyl-5-amino-1*H*-pyrazole-3-carboxylate (**49**) or its chloroderivative **52**, respectively. Similar reaction of potassium 2-cyano-4-ethoxy-4-oxobut-2-en-2-olate (**46**), which was obtained as **45** using proprionitrile, with phenylhydrazine or substituted phenylhydrazines furnished esters **50**, **53**, and **55**–**58**.

Ethyl 2-chloro-2-(2-phenylhydrazono)acetate (**47**) and its 4-chloroderivative **48** were prepared by treating the appropriate aryldiazonium salt with ethyl 2-chloroacetoacetate. Reaction of **47** or **48** with malononitrile in the presence of sodium ethoxide gave **51** and **54**, respectively. Pyrrole derivatives **59**–**65**, **67**, **69**, and **71** were prepared by heating the corresponding amines **49**–**58** with 2,5-dimethoxytetrahydrofuran in glacial acetic acid according to the Clauson−Kaas procedure.[37] Dimethylpyrroles **66**, **68**, **70**, and **72** were obtained by reaction of amines **55**–**58** with acetonylacetone in refluxing acetic acid. Lithium hydroxide hydrolysis of esters **59**–**72** at room temperature afforded the corresponding acids **73**–**86**.

The pyrazole-4-carboxylic acid **89** for the synthesis of amides **20** and **21** was prepared as depicted in Scheme 2. Reaction of 4-chlorophenylhydrazine with 2-(1-ethoxyethylidene)malononitrile in the presence of sodium ethoxide gave 5-amino-1-(4-chlorophenyl)-3-methyl-1*H*-pyrazole-4-carbonitrile (**87**), which was transformed into the corresponding pyrrole derivative **88** by reaction with 2,5-dimethoxytetrahydrofuran in glacial acetic acid. Transformation of **88** into the acid **89** was achieved by alkaline hydrolysis in refluxing ethylene glycol. Finally, carboxamides **11**–**44** were obtained through parallel solution-phase synthesis[38] by coupling acids **73**–**86** and **89** with selected amines in the presence of EDC/HOBt, using morpholinomethyl-polystyrene and polymer bound *p*-toluenesulfonic acid as scavengers for acidic and basic substances, respectively. The acidic scavenger was not used in the preparation of the *N*-piperidin-1-yl amides.

Biology. The binding affinities (K_i values) of compounds **11**–**44** for human recombinant CB_1 (hCB_1) and CB_2 (hCB_2) receptors are reported in Table 1. Tested compounds were evaluated in parallel with **2** and **7** as CB_1 and CB_2 reference compounds, respectively. The new compounds were evaluated in CB_1 and CB_2 receptor binding assays using membranes from HEK cells transfected with either the hCB_1 or hCB_2 receptor and [^{3}H]-(−)-*cis*-3-[2-hydroxy-4-(1,1-dimethylheptyl)phenyl]-*trans*-4-(3-hydroxypropyl)cyclohexanol ([^{3}H]-CP-55,940; K_d = 0.18 nM for CB_1 receptor, and K_d = 0.31 nM for CB_2 receptor) as the high affinity ligand, as described by the manufacturer (Perkin-Elmer, Italy).[39] Displacement curves were generated by incubating drugs with [^{3}H]CP-55,940 (0.14 nM for CB_1 and 0.084 nM for CB_2 binding assay). In all cases, K_i values were calculated by applying the Cheng−Prusoff equation[40] to the IC_{50} values (obtained by GraphPad) for the displacement of the bound radioligand by increasing concentrations of the test compounds. The functional activity of some of the compounds with highest affinity and selectivity at CB_1 receptors, that is, compounds **26**, **30**, and **39**, was only assessed at CB_1 receptors by studying their effects on forskolin-induced cAMP formation in mouse N18TG2 neuroblastoma cells, because this assay is well-established in our laboratory. Usually, a good agreement is observed between the affinity of agonists and inverse agonists at CB_1 receptors and their effects in this assay.[41]

Results and Discussion

Carboxamides **23**–**31**, **33**, **39**, **40**, and **44** showed high hCB_1 receptor binding affinity, with K_i values in the nanomolar range. The most potent hCB_1 ligand **30** (K_i = 5.6 nM) was comparable to the CB_1 reference compound **2** (K_i = 2.3 nM). Seven compounds (**24**, **27**, **28**, **30**, **31**, **33**, and **37**) were high affinity

Table 1. Structure, and hCB_1 and hCB_2 Receptor Affinity (K_i Values) of Derivatives **11**–**44** and Reference Compounds **1**, **2**, and **7**[a]

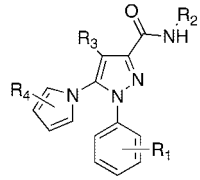

11-19, **22-44**

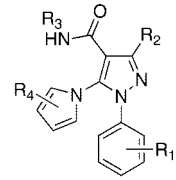

20, **21**

					hCB_1[b,d]	hCB_2[c,d]	CB_2/CB_1	
Compd	R_1	R_2	R_3	R_4	K_i[e,f]	K_i[e,f]	S.I.[g]	ALOGPs[h]
11	H		H	H	>2820	>3940	-	3.07
12	H		Me	H	>2820	>3940	-	3.20
13	H		CN	H	>2820	>3940	-	2.84
14	H		CN	H	280	3940	14.07	4.92
15	4-Cl		H	H	2820	>3940	>1.40	3.67
16	4-Cl		H	H	280	1750	6.25	4.67
17	4-Cl		Me	H	110	2180	19.82	3.76
18	4-Cl		Me	H	110	390	3.55	5.22
19	4-Cl		CN	H	2820	>3940	>1.40	3.41
20	4-Cl	Me		H	>2820	>3940	-	3.71
21	4-Cl	Me	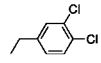	H	2820	>3940	>1.40	5.50
22	2,4-Cl_2		Me	H	1850	1730	0.94	4.31
23	2,4-Cl_2		Me	H	37	510	13.78	5.91
24	2,4-Cl_2		Me	H	56	64	1.14	5.36
25	2,4-Cl_2		Me	2,5-Me_2	38	980	25.79	4.53
26	2,4-Cl_2		Me	2,5-Me_2	28	3940	140.70	6.51
27	2,4-Cl_2		Me	2,5-Me_2	42	87	2.07	5.73
28	3,4-Cl_2		Me	H	30	20	0.67	4.29
29	3,4-Cl_2		Me	H	35	150	4.29	5.91
30	3,4-Cl_2		Me	H	5.6	1.7	0.30	5.35
31	3,4-Cl_2		Me	2,5-Me_2	28	29	1.04	4.51
32	3,4-Cl_2		Me	2,5-Me_2	280	1370	4.89	6.48
33	3,4-Cl_2		Me	2,5-Me_2	14	1.3	0.093	5.69
34	2,4-F_2		Me	H	2800	2400	0.86	3.06
35	2,4-F_2		Me	H	>2820	>3940	-	2.28
36	2,4-F_2		Me	H	2800	390	0.14	4.94
37	2,4-F_2		Me	H	1600	65	0.041	4.36

Table 1. Continued

Compd	R_1	R_2	R_3	R_4	hCB_1[b,d] K_i[e,f]	hCB_2[c,d] K_i[e,f]	CB_2/CB_1 S.I.[g]	ALOGPs[h]
38	2,4-F_2		Me	2,5-Me_2	1600	3940	2.46	3.52
39	2,4-F_2		Me	2,5-Me_2	35	3940	112.57	5.40
40	2,4-F_2		Me	2,5-Me_2	35	570	16.3	4.68
41	2,4,6-Cl_3		Me	H	1800	>3940	>2.19	4.74
42	2,4,6-Cl_3	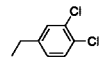	Me	H	280	>3940	>14.07	6.42
43	2,4,6-Cl_3		Me	2,5-Me_2	110	3940	35.82	4.98
44	2,4,6-Cl_3		Me	2,5-Me_2	28	390	13.93	6.19
1[i,l]	-	-	-	-	12	790	65.83	5.47
2[i,l]	-	-	-	-	2.3	112	48.70	5.30
7[k,l]	-	-	-	-	>2820	5.4	<0.002	7.00

[a] Data represent mean values for at least three separate experiments performed in duplicate and are expressed as K_i (nM). Standard error of means (SEM) are not shown for the sake of clarity and were never higher than 5% of the means. [b] hCB_1: human CB_1 receptor. [c] hCB_2: human CB_2 receptor. [d] For both receptor binding assays, the new compounds were tested using membranes from HEK cells transfected with either the hCB_1 or hCB_2 receptor and [^{3}H]-(−)-*cis*-3-[2-hydroxy-4-(1,1-dimethylheptyl)-phenyl]-*trans*-4-(3-hydroxy-propyl)-cyclohexanol ([^{3}H]CP-55,940). [e] K_i: equilibrium dissociation constant, which is the concentration of the competing ligand that will bind to half the binding sites at equilibrium, in the absence of radioligand or other competitors. [f] IC_{50}: the concentration of competitor that competes for half of the specific binding. This is the measure of the competitor's potency at interacting with the receptor against the radioligand. IC_{50} values are shown in Table 3S of Supporting Information. [g] S.I.: CB_1 selectivity index was calculated as K_i (CB_2)/ K_i (CB_1) ratio. [h] Values calculated at the following website: http://www.vcclab.org. [i] Compound **1**: rimonabant, CB_1 reference compound. [j] Compound **2**: AM251, CB_1 reference compound. [k] Compound **7**: SR144528, CB_2 reference compound. [l] The binding affinities of reference compounds were evaluated in parallel with compounds **11**–**44** under the same conditions.

ligands for the CB_2 receptor. Compound **30** (K_i = 1.7 nM) and **33** (K_i = 1.3 nM) showed K_i values even lower than that of the CB_2 reference compound **7** (K_i = 5.4 nM). The CB_1 selectivity indexes, calculated as K_i (CB_2)/K_i (CB_1) ratio, ranged from 140.7 (**26**) to 0.04 (**37**).

Affinity of 11–21 for the hCB_1 Receptor. Derivatives **11**–**21** bearing a phenyl (**11**–**14**) or 4-chlorophenyl (**15**–**21**) group at position 1 of the pyrazole nucleus displayed low affinity for both receptor subtypes, independently of the substituent at position 4 (H, Me or CN). The 4-methyl derivative **17** showed higher affinity for the hCB_1 than **15** and the corresponding 4-cyano derivative **19** (the isomeric carboxamide **20** showed no affinity). On the other hand, compounds **14** and **16** showed higher affinity than **15**. logP calculations indicated some correlation between the hCB_1 receptor affinity of **11**–**21** and their lipophilic nature (Table 1). These preliminary results prompted us to design new compounds characterized by (i) two or three halogen atoms at the 1-phenyl ring, (ii) replacement of *N*-piperidin-1-yl substituent of **1** with either cyclohexyl or 3,4-dichlorobenzyl moiety, (iii) a methyl group at position 4 of pyrazole, and (iv) the 2,5-dimethyl substitution of the 5-pyrrole nucleus.

Affinity of 22–44 for the hCB_1 Receptor. Derivatives **23**–**33**, bearing two chlorine atoms at the positions 2,4 or 3,4 of the 1-phenyl ring, showed high affinity for the hCB_1 receptor. The 1-(2,4-dichlorophenyl)-5-(2,5-dimethylpyrrol-1-yl)pyrazoles **26** and **27** were as potent as the pyrrole counterparts **23** and **24**; **25** showed higher affinity (49-fold) than **22**. Compound **26** (S.I. = 140.7) was the most selective ligand for the hCB_1 receptor within the series and was 2.9-fold more selective than **2** for this receptor subtype. The 1-(3,4-dichlorophenyl)derivatives **28**–**33** also showed high hCB_1 affinity. The *N*-cyclohexylcarboxamide **30**, the most potent hCB_1 ligand (K_i = 5.6 nM), showed receptor affinity comparable to that of **2** (K_i = 2.3 nM). Among the 1-(2,4-difluorophenyl)- **34**–**40** and 1-(2,4,6-trichlorophenyl) derivatives **41**–**44**, only 2,5-dimethylpyrroles **39**, **40**, and **44** showed high hCB_1 affinity.

Affinity of 22–44 for the hCB_2 Receptor. The hCB_2 receptor affinity was correlated with the nature of the *N*-substituent at the 3-carboxamide. The 3-(*N*-cyclohexyl)carboxamides **24**, **27**, **30**, **33**, **37**, **40**, and **44** showed higher affinity for the hCB_2 subtype compared to compounds bearing different amide moieties. Conversely, the *N*-(3,4-dichlorobenzyl)carboxamides showed weaker hCB_2 affinity. Compounds **30** (K_i = 1.7 nM) and **33** (K_i = 1.3 nM) showed higher affinity for hCB_2 than the reference compound **7** (K_i = 5.4 nM); however, because of the concomitant high hCB_1 affinity, these ligands were poorly selective.

The low receptor affinity displayed by the trichlorophenyl derivatives (with the exception of **44** for hCB_1) suggested that the chlorine atoms at positions 2 and 2′ could force the 1-phenyl ring to adopt an unfavorable binding conformation.

CB_2/CB_1 Selectivity. The CB_1 selectivity correlated well with both 1-(2,4-dihalosubstituted)phenyl ring and 2,5-dimethylpyrrole nucleus. The *N*-(3,4-dichlorobenzyl)carboxamides **26** and **39** showed the highest CB_1 selectivity (CB_2/CB_1 S.I. = 140.7 and 112.6, respectively). Also, the CB_2 selectivity was affected by the substituent at the carboxamide nitrogen. In particular, among the 1-(dihalophenyl)pyrazoles, *N*-cyclohexylcarboxamides generally exhibited high CB_2 selectivity; **33** and **37** were the most CB_2 selective compounds (CB_2/CB_1 S.I. = 0.09 and 0.04, respectively; Chart 2).

Functional Activity at Mouse CB_1 Receptors. Compounds **26**, **39**, and, particularly, **30** behaved as inverse agonists

Scheme 1. Synthesis of 1-Phenyl-5-(1*H*-pyrrol-1-yl)-1*H*-pyrazole-3-carboxamides **11**–**19** and **22**–**44**[a]

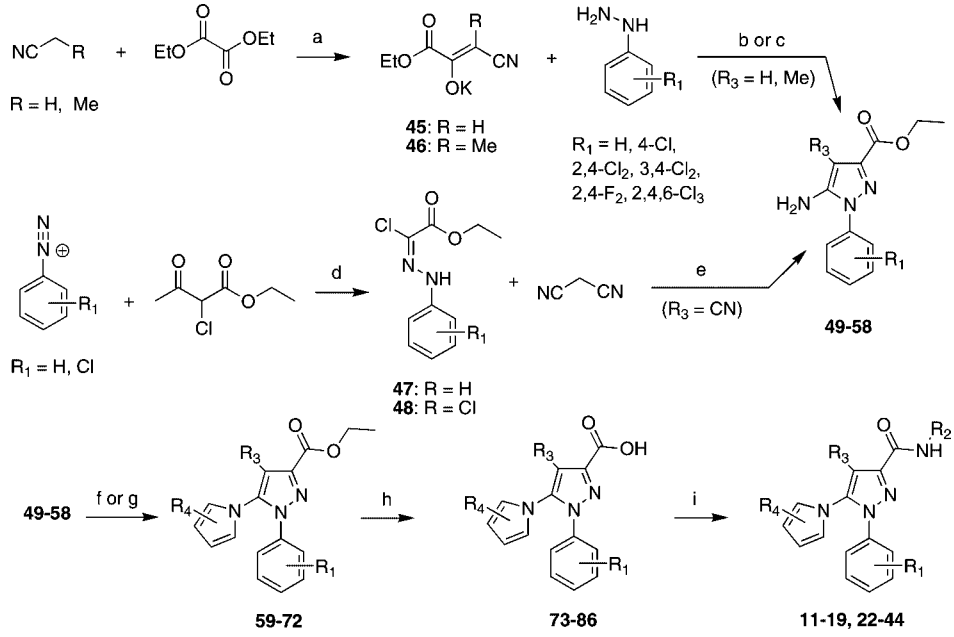

49 $R_1 = R_3 = H$
50 $R_1 = H$, $R_3 = Me$
51 $R_1 = H$, $R_3 = CN$
52 $R_1 = 4\text{-Cl}$, $R_3 = H$
53 $R_1 = 4\text{-Cl}$, $R_3 = Me$
54 $R_1 = 4\text{-Cl}$, $R_3 = CN$
55 $R_1 = 2,4\text{-Cl}_2$, $R_3 = Me$
56 $R_1 = 3,4\text{-Cl}_2$, $R_3 = Me$
57 $R_1 = 2,4\text{-F}_2$, $R_3 = Me$
58 $R_1 = 2,4,6\text{-Cl}_3$, $R_3 = Me$
59, **73** $R_1 = R_3 = R_4 = H$
60, **74** $R_1 = R_4 = H$, $R_3 = Me$
61, **75** $R_1 = R_4 = H$, $R_3 = CN$
62, **76** $R_3 = R_4 = H$, $R_1 = 4\text{-Cl}$
63, **77** $R_1 = 4\text{-Cl}$, $R_3 = Me$, $R_4 = H$
64, **78** $R_1 = 4\text{-Cl}$, $R_3 = CN$, $R_4 = H$
65, **79** $R_1 = 2,4\text{-Cl}_2$, $R_3 = Me$, $R_4 = H$
66, **80** $R_1 = 2,4\text{-Cl}_2$, $R_3 = Me$, $R_4 = 2,5\text{-Me}_2$
67, **81** $R_1 = 3,4\text{-Cl}_2$, $R_3 = Me$, $R_4 = H$
68, **82** $R_1 = 3,4\text{-Cl}_2$, $R_3 = Me$, $R_4 = 2,5\text{-Me}_2$
69, **83** $R_1 = 2,4\text{-F}_2$, $R_3 = Me$, $R_4 = H$
70, **84** $R_1 = 2,4\text{-F}_2$, $R_3 = Me$, $R_4 = 2,5\text{-Me}_2$
71, **85** $R_1 = 2,4,6\text{-Cl}_3$, $R_3 = Me$, $R_4 = H$
72, **86** $R_1 = 2,4,6\text{-Cl}_3$, $R_3 = Me$, $R_4 = 2,5\text{-Me}_2$

[a] Reagents and conditions: (a) 18-crown-6, *t*-BuOK, THF, 60 °C, 30 min; (b) R_1-phenylhydrazine (R_1 = H, 2,4,6-Cl_3), 37% HCl, ethanol, reflux, 6 h, 40–50%; (c) R_1-phenylhydrazine (R_1 = 2,4-Cl_2, 3,4-Cl_2, 2,4-F_2) hydrochloride, ethanol, reflux, 2 h, 47–89%; (d) MeCOOH/MeCOONa (1:1), ethanol, water, −5 °C, 4 h; (e) EtONa, anhydrous ethanol, room temp, 3 h, 65–88%; (f) 2,5-dimethoxytetrahydrofuran, glacial acetic acid, reflux 1 h, 60–96%; (g) acetonylacetone, glacial acetic acid, reflux 1.5 h, 65–90%; (h) LiOH, tetrahydrofuran, water, room temp, overnight, 83–99%; (i) amine, EDC/HOBt, dichloromethane, room temp, overnight, 30–93%.

Scheme 2. Synthesis of 1-Phenyl-5-(1*H*-pyrrol-1-yl)-1*H*-pyrazole-4-carboxamides **20** and **21**[a]

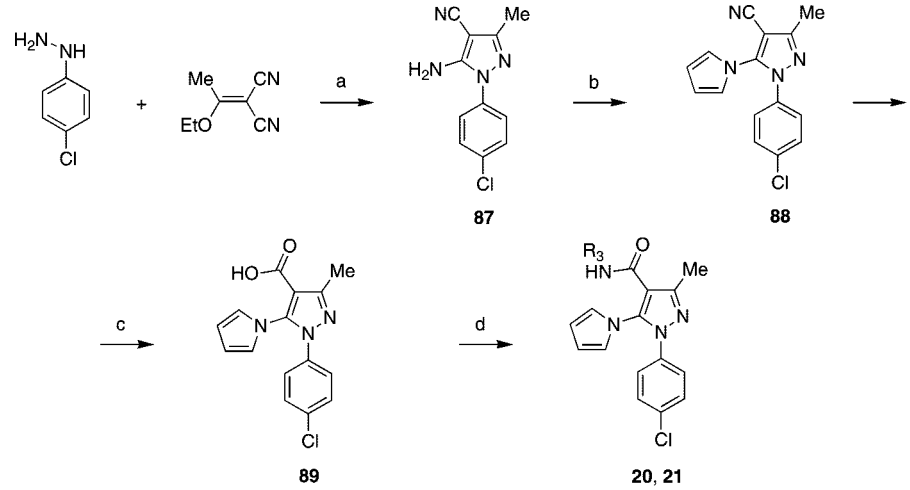

[a] Reagents and conditions: (a) EtONa, anhydrous ethanol, reflux, 1 h; (b) 2,5-dimethoxytetrahydrofuran, glacial acetic acid, reflux, 1 h; (c) 3 N NaOH, ethylene glycole, reflux, 24 h; (d) amine, EDC/HOBt, dichloromethane, room temp, 40–43%.

inasmuch as they stimulated forskolin-induced cAMP formation by N18TG2 cells, much in the same way as the previously reported CB_1 inverse agonist **1** (Figure 1A,B). The efficacy of the three compounds seems to reflect their affinity at CB_1 receptors (Table 1), because compounds **26** (EC_{50} ~25 nM) and **39** (EC_{50} > 60 nM) were significantly less efficacious than compound **30** (EC_{50} ~1 nM), and their inhibition of forskolin-induced cAMP formation was only statistically significant at the highest dose tested (200–300 nM). Indeed, the lack of effect of these two compounds at the two lowest doses might be attributed to neutral antagonism or lack of functional activity.

The stimulation of cAMP formation by the most potent CB_1 agonist among the presently reported compounds, that is, compound **30**, was (a) dose-related, (b) observed also in the absence of forskolin, and (c) not observed in the presence of the CB_1 agonist WIN55,212-2, which instead inhibited forskolin-

Chart 2. Key Structural Elements for CB_1 and CB_2 Selectivity

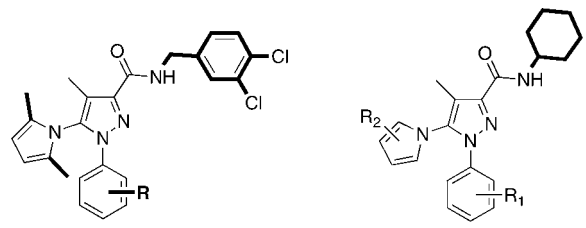

CB_1 selective
26: R = 2,4-Cl_2
39: R = 2,4-F_2

CB_2 selective
33: R_1 = 3,4-Cl_2, R_2 = 2,5-Me_2
37: R_1 = 2,4-F_2, R_2 = H

induced cAMP formation by N18TG2 cells (Figure 1). Compound **30**, at a per se inactive dose (0.1 nM), also antagonized the effect of WIN55,212-2 on forskolin-induced cAMP formation (Figure 1A).

To elucidate other factors behind the binding affinity of the above-discussed derivatives, molecular docking and MD simulations were performed at a homology model of hCB_1 receptor built using bovine rhodopsin crystal structure as a template.[42] Details of the model building are given in the Experimental Section.

Docking Studies and MD Simulations. To investigate the ligand recognition site and rationalize SARs, we performed docking studies of the highly active hCB_1 ligands **1**, **26**, and **30** using our hCB_1 receptor model. The most favorable binding locations and orientations of **1**, **26**, and **30** were determined using GOLD 3.1.[43,44] Consistency with SARs and site-mutagenesis data were taken into account in the choice of the best ligand binding mode.

Mutation data indicated that K3.28(192) is involved in a direct interaction with the carboxamide of **1** in WT CB_1 receptor.[45] Among the top-ranking docking conformations (fitness GOLD score range 46–52 kJ/mol), we chose that involving a H-bond between the carbonyl oxygen of both ligands and the lysine nitrogen of the receptor. This binding pose placed the 2,4- and 3,4-dichlorophenyl rings at position 1 of the pyrazole close to F3.36(200), Y5.39(275), and W5.43(279) residues, in agreement with previous combined mutation/modeling studies performed by McAllister.[46]

To take into account the protein flexibility and evaluate the dynamic stability of the predicted ligand/receptor interactions, the complexes obtained from the docking procedure were submitted to MD simulations for 400 ps at 300 K (see Experimental Section for details). Analysis of the MD trajectories showed that the three ligands assumed stable binding poses during the simulation time, as confirmed by their low rmsd ranges (1.2 Å for **1**, 1.4 Å for **26**, and 1.1 Å for **30**). Some distances between the ligands and receptor key residues were also stable throughout the whole simulation period and accounted for their high hCB_1 affinity. The binding of **1**, **26** (Figure 2), and **30** (Figure 3) occurred in the upper region of the helical bundle, and the ligands occupied the same area (approximately) of the binding cavity. The structural correspondence between the receptor-bound conformations of **1** and **30** inside the hCB_1 receptor binding domain is shown in Figure 4.

In agreement with the results of Hurst and co-workers,[45,47] the carboxamide oxygen of the three ligands accepted a H-bond from K3.28(192), which in turn was involved in a salt-bridge with D6.58(366). This H-bond was maintained throughout the MD simulation with a frequency of formation of 61% for **1**, 35% for **26**, and 60% for **30**. This finding accounts for the high affinity of **1**, **26**, and **30** for the inactive state of the receptor, thus explaining their inverse agonist activity.

The H-bonding analysis also showed the presence of an additional H-bond between the ligand carboxamide NH and the S7.39(383) OH oxygen, with an average occupancy of 5% for **1**, 22% for **26**, and 7% for **30**. An interesting difference between the three compounds is that the carboxamide NH of **26** is moderately (22%) occupied by H-bonding with S7.39(383) (Figure 2), whereas the same NH of **1** and **30** interacts only sporadically with S7.39(383) (5% and 7%, respectively). The latter result is substantiated by the recent site-directed mutation data from Kapur and co-workers, which showed that the binding of **1** does not change when amino acid S7.39(383) is mutated into alanine.[48] In contrast, compound **26** interacts weakly with K3.28(192) (35%) compared to **1** and **30** and, at the same time, forms a weak interaction with S7.39(383) (22%). Thus, **26** should have a nearly equal preference for inactive and active state of the receptor and, consequently, should behave as a neutral antagonist, according with the above-described functional studies on mouse CB_1 receptors.

N-Substituent of carboxamide well fitted in a pocket formed by the lipophilic N1.31(116), I1.34(119), F2.57(170), F2.61(174), F2.64(177), and A7.36(380) residues. In particular, the 3,4-dichlorobenzyl ring of **26** was involved in π-stacking interactions with both F2.61(174) and F2.64(177) aromatic rings, while the 2,4-dichlorophenyl ring formed hydrophobic interactions with a pocket made up by the residues L3.29(193), I6.54(362), M6.55(363), and V6.59(367). The 2,5-dimethylpyrrole ring directly stacked with both W5.43(279) and W6.48(356) residues and placed the two methyls in close contact with the hydrophobic residues L6.51(359) and V3.32(196), respectively. The methyl groups at positions 2 and 5 of the pyrrole ring showed a positive effect on the binding affinity. This result was consistent with a nice accommodation of the 2,5-dimethylpyrrole nucleus into a tiny hydrophobic pocket delimited by L6.51(359) and V3.32(196).

Both the 3,4-dichlorophenyl ring and pyrrole nucleus of **30** had direct aromatic stacking interactions with W5.43(279), Y5.39(275), and W6.48(356) residues. As depicted in Figure 4, these residues interacted in the same way with the 2,4-dichlorophenyl and the 4-chlorophenyl rings of **1**. The ligand bound the aromatic residue-rich TM3-4-5-6 region of the CB_1 receptor (residues F3.36(200), Y5.39(275), F5.42(278), W5.43(279), and W6.48(356)), colored magenta in Figures 2−4, and formed a large aromatic cluster in the minimized complex. The $\pi-\pi$ interactions were consistent with the affinity trend of the tested compounds. In fact, the electron-deficient halogenated phenyl rings would realize favorable aromatic stacking interactions with the electron-rich W5.43(279), Y5.39(275), and W6.48(356) residues. These results were in agreement with chimeric and site-mutagenesis studies. Studies on chimeric CB_1/CB_2 receptors demonstrated that the region delineated by TM4 and TM5 was crucial for the high-affinity binding of **1** (EL2 did not affect its binding).[49] Recently, McAllister reported that mutating the aromatic residues F3.36(200), W5.43(279), and W6.48(356) of CB_1 receptor with alanine resulted in a significant loss of affinity.[46] This finding highlighted the role of these native residues for the binding affinity of **1**.

Conclusions

We have described the synthesis of new 1-aryl-5-(1*H*-pyrrol-1-yl)pyrazole-3-carboxamides based on the bioisosteric replacement of the 4-chlorophenyl group of **1** with a pyrrole nucleus. In hCB_1 and hCB_2 receptor binding affinity assays, several

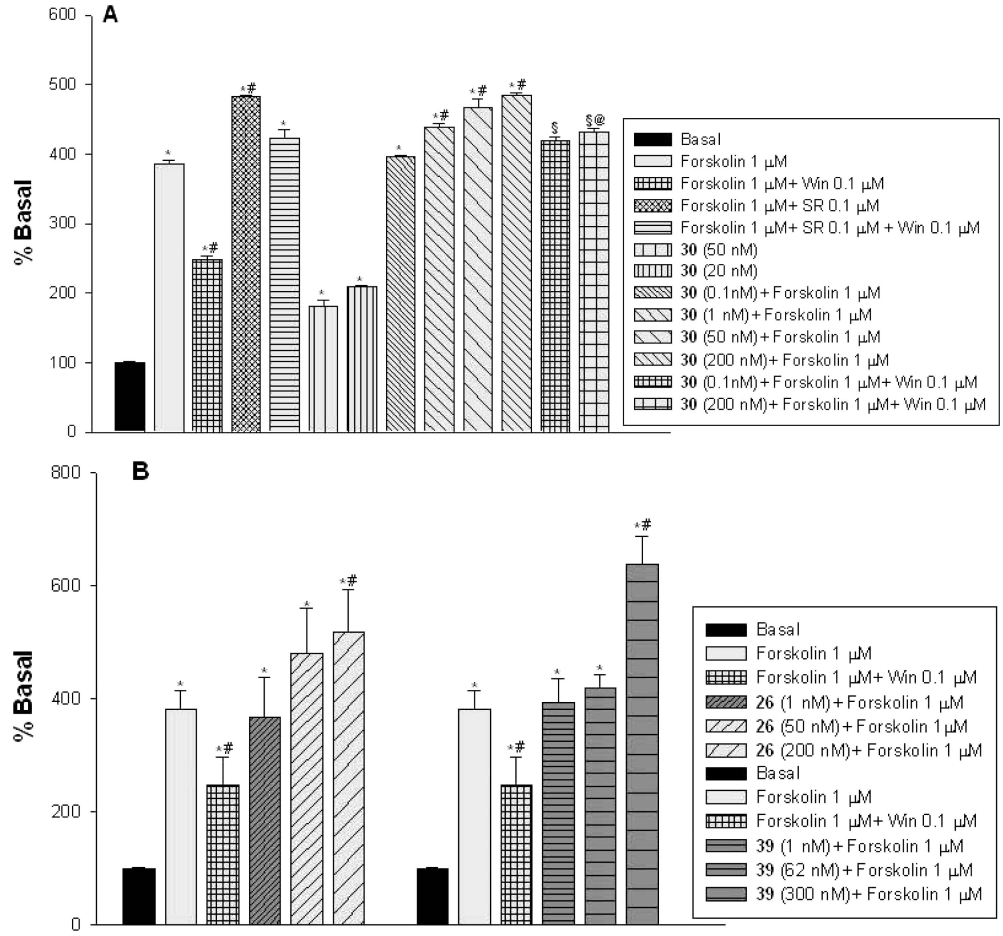

Figure 1. Forskolin-induced cAMP formation by compounds **30** (A) and **26** and **39** (B). Cyclic AMP assays were performed on intact confluent N18TG2 cells. The data for compounds **26** and **39** were obtained in the presence of forskolin 1 μM. The data for compound **30** were obtained both in the absence and presence of forskolin and both in the absence and presence of the CB_1 agonist WIN55,212-2 (Win, 100 nM), whose effect is also shown. The effect of the CB_1 receptor inverse agonist/antagonist, SR141716A (SR), is also shown. $^{\#}P < 0.05$ vs forskolin; $^{\S}P < 0.05$ vs Win + Forskolin; $^{@}P < 0.05$ vs **30** + Forskolin (200 nM).

carboxamides (**23**–**31**, **33**, **39**, **40**, and **44**) showed K_i values only 1 order of magnitude higher than that of **2**, taken in this study as a reference compound. Compound **26** was the most selective ligand for the hCB_1 receptor (S.I. = 140.7, 2.9-fold higher than **2**). The *N*-cyclohexylcarboxamide **30** ($K_i = 5.6$ nM), the most potent hCB_1 ligand, showed receptor affinity comparable to that of **2** ($K_i = 2.3$ nM) and behaved as an inverse agonist in the cAMP assay ($EC_{50} \sim 1$ nM). At CB_2 receptors, compounds **30** ($K_i = 1.7$ nM) and **33** ($K_i = 1.3$ nM) showed higher binding affinities than that of the hCB_2 reference compound **7** ($K_i = 5.4$ nM). However, because of the concomitant high hCB_1 affinity, these ligands were poorly selective. Compound **37**, endowed with low hCB_1 affinity, proved to be the most selective hCB_2 ligand (CB_1 S.I. = 0.04). Docking studies and MD simulations of **1** and the most selective (**26**) and potent (**30**) hCB_1 ligands were undertaken using an inactive state model of hCB_1 receptor. The binding of **1**, **26**, and **30** occurred in the upper region of the helical bundle, where the 1-phenyl and the 5-pyrrole/5-phenyl rings of these ligands formed aromatic stacking interactions. The 2,5-dimethylpyrrole moiety of **26** positively affected the hCB_1 binding affinity as a result of a nice accommodation into a tiny hydrophobic pocket. Carboxamide *N*-substituent well fitted in a pocket formed by lipophilic residues. The ability of the carboxamide to form a H-bond with K3.28(192) accounted for the high affinity for hCB_1 receptor inactive state and the inverse agonist activity of **26** and **30**. In conclusion, the bioisosteric replacement of the 4-chlorophenyl group of **1** with a pyrrole ring furnished new potent hCB_1 inverse agonists. Not unexpectedly, fine chemical modifications of the same molecular scaffold led to potent hCB_2 ligands as well. However, the issue of selectivity still has to be addressed for this new class of cannabinergic agents.

Experimental Section

Chemistry. Melting points (mp) were determined on a Büchi 510 apparatus, a Kofler hot stage apparatus or using a Mettler FPI apparatus (2 °C/min) and are uncorrected. Infrared spectra (IR) were run on a SpectrumOne FT spectrophotometer or on a Perkin-Elmer 1600 spectrophotometer. Band position and absorption ranges are given in cm^{-1}. Proton nuclear magnetic resonance (^1H NMR) spectra were recorded on Bruker 200 and 400 MHz FT spectrometers in the indicated solvent. Chemical shifts are expressed in δ units (ppm) from tetramethylsilane. Mass spectral data were determined with an Agilent 1100 spectrometer LC/MSD (electrospray) VL (G1946C). Column chromatography was performed on columns packed with alumina from Merck (70–230 mesh) or silica gel from Merck (70–230 mesh). Aluminum oxide TLC cards from Fluka (aluminum oxide precoated aluminum cards with fluorescent indicator at 254 nm) and silica gel TLC cards from Fluka (silica gel precoated aluminum cards with fluorescent indicator at 254 nm) were used for thin layer chromatography (TLC). Developed plates were visualized by a Spectroline ENF 260C/F UV apparatus. Organic solutions were dried over anhydrous sodium sulfate. Evaporation of the solvents was carried out on a Büchi Rotavapor R-210 equipped with a Büchi V-850 vacuum controller and Büchi

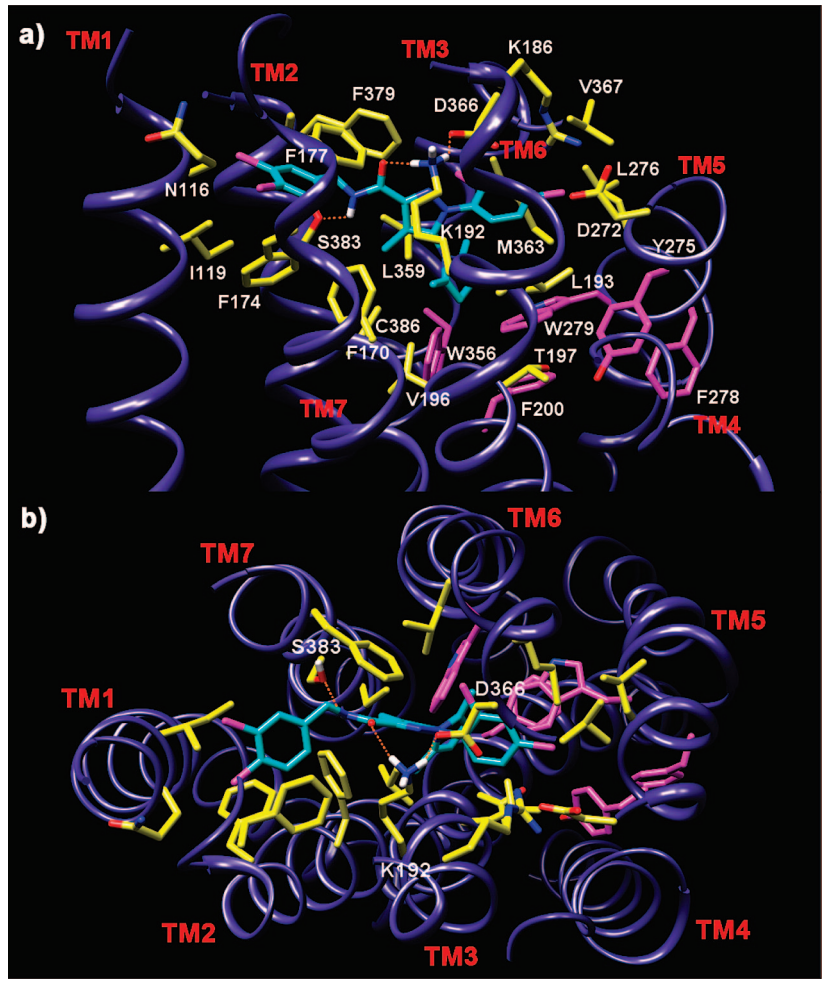

Figure 2. Complex of the hCB_1 receptor with compound **26**. (a) View from the plane of the cell membrane of the **26**/hCB_1 complex. (b) View from outside the cell of the **26**/hCB_1complex. Only amino acids located within 4 Å distance from the ligand (cyan) are shown in yellow and labeled. Residues that form part of the aromatic cluster complex with ligand are colored in magenta. H-bonds are indicated by dashed orange lines.

V-700 and V-710 vacuum pumps. Elemental analyses were found within ±0.4% of the theoretical values. Büchi Syncore reactor was used for parallel synthesis, filtration, and evaporation.

Synthesis of Amides 11–44. General Procedure. To a solution of the appropriate acid, **73**–**86** or **89** (1 mmol), in dichloromethane, kept at 0 °C, EDC hydrochloride (1.2 mmol), and HOBt (1.0 mmol) were added followed by the appropriate amine (1.5 mmol). The solution was allowed to warm up at room temperature and placed in the Büchi Syncore reactor. The reaction was stirred at 300 rpm overnight and then morpholinomethyl-polystyrene (3 equiv/mol) was added. After 1 h at room temperature, polymer bound *p*-toluensulfonic acid (3 equiv/mol) was added and the mixture was stirred for 24 h at room temperature. The mixture was filtered and the solution was evaporated to dryness under reduced pressure. Purification of the crude product by crystallization from dichloromethane furnished the carboxamide **11**–**44**.

***N*-Piperidin-1-yl 1-Phenyl-5-(1*H*-pyrrol-1-yl)-1*H*-pyrazole-3-carboxamide (11).** Yield 57% (pink solid), mp 166–168 °C. ^{1}H NMR ($CDCl_3$): δ 1.56–1.58 (m, 2H), 1.80–1.90 (m, 4H), 3.28–3.32 (m, 4H), 6.23–6.24 (m, 2H), 6.58–6.59 (m, 2H), 6.92 (s, 1H), 7.11–7.16 (m, 2H), 7.33–7.36 (m, 3H), 8.50 ppm (broad s, 1H). IR: ν 1682 cm^{-1}. MS *m*/*z*: 336 $[M + 1]^+$ (100), 358 $[M + 23]^+$ (30), 693 $[2M + 23]^+$ (90). Anal. ($C_{19}H_{21}N_5O$ (335.40)) C, H, N.

***N*-Piperidin-1-yl 4-Methyl-1-phenyl-5-(1*H*-pyrrol-1-yl)-1*H*-pyrazole-3-carboxamide (12).** Yield 62% (beige solid), mp 188–190 °C. ^{1}H NMR ($CDCl_3$): δ 1.48–1.68 (m, 2H), 1.75–1.89 (m, 4H), 2.24 (s, 3H), 3.96–4.11 (m, 4H), 6.28–6.29 (m, 2H), 6.58–6.59 (m, 2H), 7.04–7.09 (m, 2H), 7.27–7.30 (m, 3H), 7.83 ppm (broad s, 1H). IR: ν 1681 cm^{-1}. MS *m*/*z*: 350 $[M + 1]^+$ (100), 372 $[M + 23]^+$ (20), 721 $[2M + 23]^+$(50). Anal. ($C_{20}H_{23}N_5O$ (349.43)) C, H, N.

***N*-Piperidin-1-yl 4-Cyano-1-phenyl-5-(1*H*-pyrrol-1-yl)-1*H*-pyrazole-3-carboxamide (13).** Yield 31% (white solid), mp 242–243 °C. ^{1}H NMR ($CDCl_3$): δ 1.42–1.48 (m, 2H), 1.77–1.91 (m, 4H), 3.09–3.25 (m, 4H), 6.29–6.31 (m, 2H), 6.66–6.68 (m, 2H), 7.15–7.21 (m, 2H), 7.40–7.42 (m, 3H), 8.25 ppm (broad s, 1H). IR: ν 1695, 2243 cm^{-1}. MS *m*/*z*: 361 $[M + 1]^+$ (100), 383 $[M + 23]^+$ (60). Anal. ($C_{20}H_{20}N_6O$ (360.41)) C, H, N.

***N*-3,4-Dichlorobenzyl 4-Cyano-1-phenyl-5-(1*H*-pyrrol-1-yl)-1*H*-pyrazole-3-carboxamide (14).** Yield 41% (white solid), mp 152–154 °C. ^{1}H NMR ($CDCl_3$): δ 4.58 (d, J = 6.31 Hz, 2H), 6.31 (s, 2H), 6.70 (s, 2H), 7.13–7.21 (m, 3H), 7.37–7.42 ppm (m, 5H). IR: ν 1686, 2242 cm^{-1}. MS *m*/*z*: 436 $[M + 1]^+$ (40), 459 $[M + 23]^+$ (100). Anal. ($C_{22}H_{15}Cl_2N_5O$ (436.29)) C, H, Cl, N.

***N*-Piperidin-1-yl 1-(4-Chlorophenyl)-5-(1*H*-pyrrol-1-yl)-1*H*-pyrazole-3-carboxamide (15).** Yield 30% (beige solid), mp 175–176 °C. ^{1}H NMR ($CDCl_3$): δ 1.51–1.53 (m, 2H), 1.80–1.88 (m, 4H), 3.19–3.65 (m, 4H), 6.25–6.27 (m, 2H), 6.57–6.59 (m, 2H), 6.93 (s, 1H), 7.05 (d, J = 8.80, 2H), 7.30 (d, J = 8.80, 2H), 8.31 ppm (broad s, 1H). IR: ν 1686 cm^{-1}. MS *m*/*z*: 370 $[M + 1]^+$ (100), 392 $[M + 23]^+$ (30), 761 $[2M + 23]^+$ (50). Anal. ($C_{19}H_{20}ClN_5O$ (369.85)) C, H, Cl, N.

***N*-Cyclohexyl 1-(4-Chlorophenyl)-5-(1*H*-pyrrol-1-yl)-1*H*-pyrazole-3-carboxamide (16).** Yield 68% (white solid), mp 119–122 °C. ^{1}H NMR ($CDCl_3$): δ 1.17–1.46 (m, 6H), 1.50–1.78 (m, 2H), 1.98–2.03 (m, 2H), 3.93–3.98 (m, 1H), 6.25–6.27 (m, 2H),

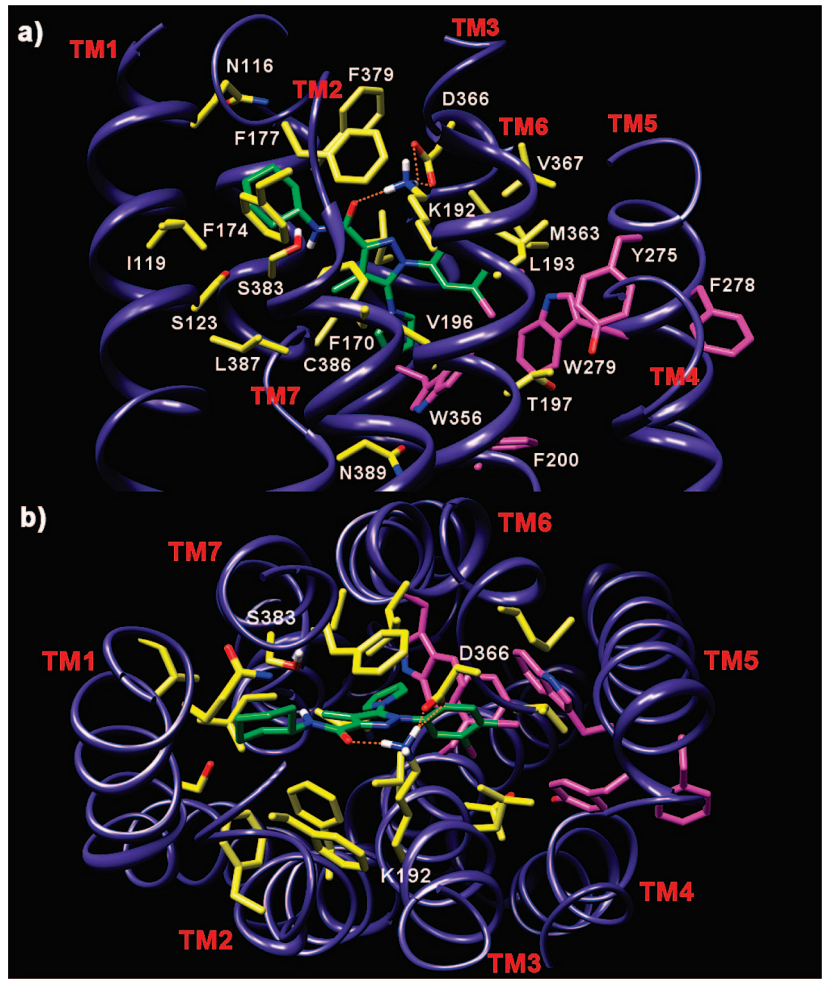

Figure 3. Complex of the hCB_1 receptor with the potent inverse agonist **30**. (a) View from the plane of the cell membrane of the **30**/hCB_1 complex. (b) View from outside the cell of the **30**/hCB_1 complex. Only amino acids located within 4 Å distance from the ligand (green) are shown in yellow and labeled. Residues that form part of the aromatic cluster complex with ligand are colored in magenta. H-bonds are indicated by dashed orange lines.

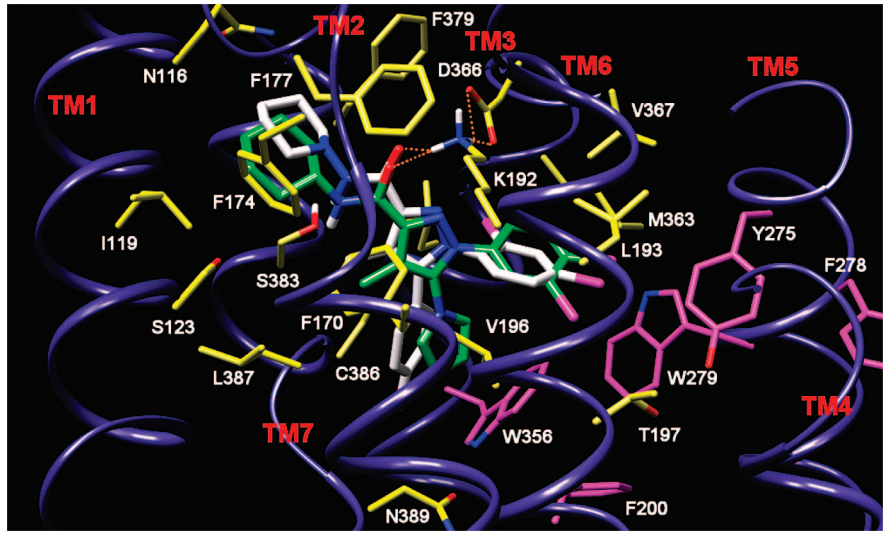

Figure 4. Structural correspondence of the receptor-bound conformations of **1** (white) and **30** (green) inside the hCB_1 receptor binding domain. Only amino acids located within 4 Å distance from the ligands are shown in yellow and labeled. Residues that form part of the aromatic cluster complex with ligand are colored in magenta. H-bonds are indicated by dashed orange lines.

6.58–6.61 (m, 2H), 6.79 (d, J = 8.32 Hz, 1H), 6.90 (s, 1H), 7.04 (d, J = 8.80 Hz, 2H), 7.31 ppm (d, J = 8.80 Hz, 2H). IR: ν 1664 cm^{-1}. MS *m/z*: 369 $[M + 1]^+$ (60), 391 $[M + 23]^+$ (80), 759 $[2M + 23]^+$. Anal. ($C_{20}H_{21}ClN_4O$ (368.86)) C, H, Cl, N.

***N*-Piperidin-1-yl 1-(4-Chlorophenyl)-4-methyl-5-(1*H*-pyrrol-1-yl)-1*H*-pyrazole-3-carboxamide (17).** Yield 65% (brown solid), mp 193–195 °C. ^1H NMR ($CDCl_3$): δ 1.44–1.50 (m, 2H), 1.68–1.81 (m, 4H), 2.24 (s, 3H), 2.90–2.92 (m, 4H), 6.29–6.31 (m, 2H),

6.56–6.58 (m, 2H), 6.98 (d, J = 8.80 Hz, 2H), 7.26 (d, J = 8.80 Hz, 2H), 7.76 ppm (broad s, 1H). IR: ν 1681 cm^{-1}. MS m/z: 384 $[M + 1]^+$ (100), 406 $[M + 23]^+$ (60), 789 $[2M + 23]^+$ (40). Anal. ($C_{20}H_{22}ClN_5O$ (383.87)) C, H, Cl, N.

***N*-Cyclohexylmethyl 1-(4-Chlorophenyl)-4-methyl-5-(1*H*-pyrrol-1-yl)-1*H*-pyrazole-3-carboxamide (18).** Yield 73% (white solid), mp 148–150 °C. ^{1}H NMR ($CDCl_3$): δ 0.96–1.17 (m, 2H), 1.22–1.28 (m, 4H), 1.57–1.82 (m, 5H), 2.25 (s, 3H), 3.27 (t, J = 6.29 Hz, 2H), 6.30–6.32 (m, 2H), 6.58–6.59 (m, 2H), 7.01 (d, J = 8.80 Hz, 2H), 7.05 (broad s, 1H), 7.26 ppm (d, J = 8.80 Hz, 2H). IR: ν 1664 cm^{-1}. MS m/z: 397 $[M + 1]^+$ (100), 419 $[M + 23]^+$ (60), 815 $[2M + 23]^+$ (30). Anal. ($C_{22}H_{25}ClN_4O$ (396.91)) C, H, Cl, N.

***N*-Piperidin-1-yl 1-(4-Chlorophenyl)-4-cyano-5-(1*H*-pyrrol-1-yl)-1*H*-pyrazole-3-carboxamide (19).** Yield 41% (white solid), mp 300–301 °C. ^{1}H NMR ($CDCl_3$): δ 1.23–1.53 (m, 2H), 1.71–1.77 (m, 4H), 2.88–2.93 (m, 4H), 6.34 (s, 2H), 6.68 (s, 2H) 7.15 (t, J = 8.80 Hz, 2H), 7.38 (d, J = 8.80 Hz, 2H), 7.54 ppm (broad s, 1H). IR: ν 1664, 2243 cm^{-1}. MS m/z: 395 $[M + 1]^+$ (100), 417 $[M + 23]^+$ (80), 811 $[2M + 23]^+$ (90). Anal. ($C_{20}H_{19}ClN_6O$ (394.86)) C, H, Cl, N.

***N*-Piperidin-1-yl 1-(4-Chlorophenyl)-3-methyl-5-(1*H*-pyrrol-1-yl)-1*H*-pyrazole-4-carboxamide (20).** Yield 40% (white solid) mp 118–121 °C. ^{1}H NMR ($CDCl_3$): δ 1.30–1.33 (m, 2H), 1.50–1.60 (m, 4H), 2.43 (s, 3H), 2.46–2.48 (m, 2H), 2.56–2.88 (m, 2H), 6.42 (s, 2H), 6.70 (s, 2H), 6.96 (broad s, 1H), 7.03 (d, J = 8.80 Hz, 2H), 7.25 ppm (d, J = 8.80 Hz, 2H). IR: ν 1617 cm^{-1}. MS m/z: 369 $[M + 1]^+$ (40), 391 $[M + 23]^+$ (100), 759 $[2M + 23]^+$(30). Anal. ($C_{20}H_{22}ClN_5O$ (383.87)) C, H, Cl, N.

***N*-3,4-Dichlorobenzyl 1-(4-Chlorophenyl)-3-methyl-5-(1*H*-pyrrol-1-yl)-1*H*-pyrazole-4-carboxamide (21).** Yield 43% (white solid) mp 123–124 °C. ^{1}H NMR ($CDCl_3$): δ 2.50 (s, 3H), 4.30 (d, J = 5.68 Hz, 2H), 5.36 (broad s, 1H), 6.37 (s, 2H), 6.69 (s, 2H), 6.91–7.15 (m, 3H), 7.23–7.33 ppm (m, 4H). IR: ν 1621 cm^{-1}. MS m/z: 460 $[M + 1]^+$ (10), 482 $[M + 23]^+$ (100), 498 $[M + 39]^+$(40). Anal. ($C_{22}H_{17}Cl_3N_4O$ (459,76)) C, H, Cl, N.

***N*-Piperidin-1-yl 1-(2,4-Dichlorophenyl)-4-methyl-5-(1*H*-pyrrol-1-yl)-1*H*-pyrazole-3-carboxamide (22).** Yield 74% (yellow solid), mp 171 °C. ^{1}H NMR ($CDCl_3$): δ 1.41–1.47 (m, 2H), 1.68–1.79 (m, 4H), 2.27 (s, 3H), 2.85 (t, J = 5.30 Hz, 4H), 6.13–6.18 (m, 2H), 6.53–6.55 (m, 2H), 7.13–7.29 (m, 2H), 7.45 (d, J = 1.65 Hz, 1H), 7.59 ppm (s, 1H, disappeared on treatment with D_2O). IR: ν 1681 cm^{-1}. MS m/z: 418 $[M + 1]^+$ (100). Anal. ($C_{20}H_{21}Cl_2N_5O$ (418.32)) C, H, Cl, N.

***N*-3,4-Dichlorobenzyl 1-(2,4-Dichlorophenyl)-4-methyl-5-(1*H*-pyrrol-1-yl)-1*H*-pyrazole-3-carboxamide (23).** Yield 80% (pale yellow solid), mp 140 °C. ^{1}H NMR ($CDCl_3$): δ 2.30 (s, 3H), 4.54 (d, J = 6.14 Hz, 2H), 6.17–6.19 (m, 2H), 6.55–6.57 (m, 2H), 7.15–7.28 (m, 4H), 7.36–7.45 ppm (m, 2H). IR: ν 1674 cm^{-1}. MS m/z: 517 $[M + Na]^+$ (100). Anal. ($C_{22}H_{16}Cl_4N_4O$ (494.20)) C, H, Cl, N.

***N*-Cyclohexyl 1-(2,4-Dichlorophenyl)-4-methyl-5-(1*H*-pyrrol-1-yl)-1*H*-pyrazole-3-carboxamide (24).** Yield 51% (pale yellow solid), mp 192 °C. ^{1}H NMR ($CDCl_3$): δ 1.20–1.49 (m, 6H), 1.70–1.77 (m, 2H), 1.96–2.02 (m, 2H), 2.28 (s, 3H), 3.86–4.00 (m, 1H), 6.16–6.17 (m, 2H), 6.54–6.56 (m, 2H), 6.28 (broad d, J = 8.00 Hz, 1H, disappeared on treatment with D_2O), 7.17–7.28 (m, 2H), 7.45 ppm (s, 1H). IR: ν 1662 cm^{-1}. MS m/z: 440 $[M + Na]^+$ (100). Anal. ($C_{21}H_{22}Cl_2N_4O$ (417.33)) C, H, Cl, N.

***N*-Piperidin-1-yl 1-(2,4-Dichlorophenyl)-5-(2,5-dimethyl-1*H*-pyrrol-1-yl)-4-methyl-1*H*-pyrazole-3-carboxamide (25).** Yield 50% (white solid), mp 144 °C. ^{1}H NMR ($CDCl_3$): δ 1.45–1.48 (m, 2H), 1.71–1.80 (m, 4H), 1.84 (s, 6H), 2.19 (s, 3H), 2.93 (t, J = 5.22 Hz, 4H), 5.95 (s, 2H), 6.60 (d, J = 8.56 Hz, 1H), 7.23–7.34 (m, 2H), 7.71 ppm (s, 1H, disappeared on treatment with D_2O). IR: ν 1681 cm^{-1}. MS m/z: 469 $[M + Na]^+$ (100). Anal. ($C_{22}H_{25}Cl_2N_5O$ (446.37)) C, H, Cl, N.

***N*-3,4-Dichlorobenzyl 1-(2,4-Dichlorophenyl)-5-(2,5-dimethyl-1*H*-pyrrol-1-yl)-4-methyl-1*H*-pyrazole-3-carboxamide (26).** Yield 60% (white solid), mp 132 °C. ^{1}H NMR ($CDCl_3$): δ 1.94 (s, 6H), 2.18 (s, 3H), 4.56 (d, J = 6.17 Hz, 2H), 5.79 (s, 2H), 6.74 (d, J = 8.70 Hz, 1H), 7.16–7.19 (m, 2H), 7.23–7.50 ppm (m, 3H). IR: ν 1673 cm^{-1}. MS m/z: 545 $[M + K]^+$ (100). Anal. ($C_{24}H_{20}Cl_4N_4O$ (522.25)) C, H, Cl, N.

***N*-Cyclohexyl 1-(2,4-Dichlorophenyl)-5-(2,5-dimethyl-1*H*-pyrrol-1-yl)-4-methyl-1*H*-pyrazole-3-carboxamide (27).** Yield 65% (white solid), mp 128 °C. ^{1}H NMR ($CDCl_3$): δ 1.17–1.44 (m, 6H), 1.71–1.88 (m, 2H), 1.92 (s, 6H), 1.96–2.13 (m, 2H), 2.15 (s, 3H), 3.88–3.97 (m, 1H), 5.77 (s, 2H), 6.83 (broad d, J = 8.02 Hz, 1H, disappeared on treatment with D_2O), 6.88 (d, J = 8.10 Hz, 1H), 7.15 (dd, J = 1.97 and 8.37 Hz, 1H), 7.47 ppm (d, J = 1.97 Hz, 1H). IR: ν 1667 cm^{-1}. MS m/z: 469 $[M + Na]^+$ (100). Anal. ($C_{23}H_{26}Cl_2N_4O$ (445.38)) C, H, Cl, N.

***N*-Piperidin-1-yl 1-(3,4-Dichlorophenyl)-4-methyl-5-(1*H*-pyrrol-1-yl)-1*H*-pyrazole-3-carboxamide (28).** Yield 71% (white solid), mp 165 °C. ^{1}H NMR ($CDCl_3$): δ 1.44–1.50 (m, 2H), 1.70–1.81 (m, 4H), 2.25 (s, 3H), 2.89 (t, J = 5.23 Hz, 4H), 6.36 (s, 2H), 6.59 (s, 2H), 6.71 (dd, J = 2.83 and 8.80 Hz, 1H), 7.32 (d, J = 8.80 Hz, 1H), 7.66 ppm (s, 1H). IR: ν 1683 cm^{-1}. MS m/z: 418 $[M + 1]^+$ (100). Anal. ($C_{20}H_{21}Cl_2N_5O$ (418.32)) C, H, Cl, N.

***N*-3,4-Dichlorobenzyl 1-(3,4-Dichlorophenyl)-4-methyl-5-(1*H*-pyrrol-1-yl)-1*H*-pyrazole-3-carboxamide (29).** Yield 75% (pale yellow solid), mp 170 °C. ^{1}H NMR ($CDCl_3$): δ 2.27 (s, 3H), 4.58 (d, J = 6.16 Hz, 2H), 6.36–6.37 (m, 2H), 6.60–6.62 (m, 2H), 6.71 (dd, J = 2.18 and 8.76 Hz, 1H), 7.23 (d, J = 2.66 Hz, 1H), 7.32 (d, J = 8.74 Hz, 1H), 7.36–7.45 ppm (m, 3H). IR: ν 1676 cm^{-1}. MS m/z: 517 $[M + Na]^+$ (100). Anal. ($C_{22}H_{16}Cl_4N_4O$ (494.20)) C, H, Cl, N.

***N*-Cyclohexyl 1-(3,4-Dichlorophenyl)-4-methyl-5-(1*H*-pyrrol-1-yl)-1*H*-pyrazole-3-carboxamide (30).** Yield 67% (white solid), mp 160 °C. ^{1}H NMR ($CDCl_3$): δ 1.26–1.45 (m, 6H), 1.62–1.73 (m, 2H), 1.99–2.04 (m, 2H), 2.24 (s, 3H), 3.92–3.97 (m, 1H), 6.33–6.35 (m, 2H), 6.57–6.59 (m, 2H), 6.72 (dd, J = 1.89 and 8.78 Hz, 1H), 6.83 (broad d, J = 8.23 Hz, 1H, disappeared on treatment with D_2O), 7.24 (d, J = 1.89 Hz, 1H), 7.31 ppm (d, J = 8.72 Hz, 1H). IR: ν 1663 cm^{-1}. MS m/z: 857 $[2M + Na]^+$ (100). Anal. ($C_{21}H_{22}Cl_2N_4O$ (417.33)) C, H, Cl, N.

***N*-Piperidin-1-yl 1-(3,4-Dichlorophenyl)-5-(2,5-dimethyl-1*H*-pyrrol-1-yl)-4-methyl-1*H*-pyrazole-3-carboxamide (31).** Yield 64% (white solid), mp 156 °C. ^{1}H NMR ($CDCl_3$): δ 1.42–1.45 (m, 2H), 1.68–1.77 (m, 4H), 1.93 (s, 6H), 2.16 (s, 3H), 2.87 (t, J = 5.11 Hz, 4H), 5.78 (s, 2H), 6.87 (d, J = 9.20 Hz, 1H), 7.22 (dd, J = 1.55 and 9.20 Hz, 1H), 7.49 (s, 1H), 7.66 ppm (broad s, 1H, disappeared on treatment with D_2O). IR: ν 1682 cm^{-1}. MS m/z: 446 $[M + 1]^+$ (100). Anal. ($C_{22}H_{25}Cl_2N_5O$ (446.37)) C, H, Cl, N.

***N*-3,4-Dichlorobenzyl 1-(3,4-Dichlorophenyl)-5-(2,5-dimethyl-1*H*-pyrrol-1-yl)-4-methyl-1*H*-pyrazole-3-carboxamide (32).** Yield 70% (pale yellow solid), mp 118 °C. ^{1}H NMR ($CDCl_3$): δ 1.85 (s, 6H), 2.22 (s, 3H), 4.60 (d, J = 6.13 Hz, 2H), 5.96 (s, 2H), 6.60 (dd, J = 2.12 and 8.74 Hz, 1H), 7.22–7.29 (m, 2H), 7.33–7.49 ppm (m, 3H). IR: ν 1675 cm^{-1}. MS m/z: 545 $[M + Na]^+$ (100). Anal. ($C_{24}H_{20}Cl_4N_4O$ (522.25)) C, H, Cl, N.

***N*-Cyclohexyl 1-(3,4-Dichlorophenyl)-5-(2,5-dimethyl-1*H*-pyrrol-1-yl)-4-methyl-1*H*-pyrazole-3-carboxamide (33).** Yield 79% (white solid), mp 182 °C. ^{1}H NMR ($CDCl_3$): δ 1.19–1.47 (m, 6H), 1.63–1.75 (m, 2H), 1.84 (s, 6H), 2.02–2.07 (m, 2H), 2.20 (s, 3H), 3.95–4.00 (m, 1H), 5.95 (s, 2H), 6.61 (dd, J = 2.58 and 8.82 Hz, 1H), 6.87 (broad d, J = 8.07 Hz, 1H, disappeared on treatment with D_2O), 7.22 (s, 1H), 7.32 ppm (d, J = 8.82 Hz, 1H). IR: ν 1662 cm^{-1}. MS m/z: 445 $[M + 1]^+$ (100). Anal. ($C_{23}H_{26}Cl_2N_4O$ (445.38)) C, H, Cl, N.

***N*-Piperidin-1-yl 1-(2,4-Difluorophenyl)-4-methyl-5-(1*H*-pyrrol-1-yl)-1*H*-pyrazole-3-carboxamide (34).** Yield 78% (yellow solid), mp 176 °C. ^{1}H NMR ($CDCl_3$): δ 1.39–1.47 (m, 2H), 1.60–1.79 (m, 4H), 2.28 (s, 3H), 2.85 (t, J = 5.35 Hz, 4H), 6.18–6.20 (m, 2H), 6.53–6.57 (m, 2H), 6.81–6.94 (m, 2H), 7.21–7.29 (m, 1H), 7.73 ppm (broad s, 1H, disappeared on treatment with D_2O). IR: ν 1682 cm^{-1}. MS m/z: 386 $[M + 1]^+$ (100). Anal. ($C_{20}H_{21}F_2N_5O$ (385.41)) C, H, F, N.

***N*-Morpholin-4-yl 1-(2,4-Difluorophenyl)-4-methyl-5-(1*H*-pyrrol-1-yl)-1*H*-pyrazole-3-carboxamide (35).** Yield 93% (white solid), mp 152–155 °C. ^{1}H NMR ($CDCl_3$): δ 2.12 (s, 3H), 3.65–3.80

(m, 6H), 3.88–3.95 (m, 2H), 6.19–6.21 (m, 2H), 6.56–6.57 (m, 2H), 6.81–6.90 (m, 2H), 7.14–7.21 ppm (m, 1H). IR: ν 1631 cm^{-1}. MS *m/z*: 395 $[M + Na]^+$ (100). Anal. ($C_{19}H_{19}F_2N_5O_2$ (387.38)) C, H, F, N.

***N*-3,4-Dichlorobenzyl 1-(2,4-Difluorophenyl)-4-methyl-5-(1*H*-pyrrol-1-yl)-1*H*-pyrazole-3-carboxamide (36).** Yield 85% (yellow solid), mp 124 °C. ^1H NMR ($CDCl_3$): δ 2.28 (s, 3H), 4.55 (d, J = 6.22 Hz, 2H), 6.19–6.20 (m, 2H), 6.55–6.56 (m, 2H), 6.82–6.91 (m, 2H), 7.16–7.36 (m, 3H), 7.39–7.43 ppm (m, 1H). IR: ν 1676 cm^{-1}. MS *m/z*: 484 $[M + Na]^+$ (100). Anal. ($C_{22}H_{16}Cl_2F_2N_4O$ (461.29)) C, H, Cl, F, N.

***N*-Cyclohexyl 1-(2,4-Difluorophenyl)-4-methyl-5-(1*H*-pyrrol-1-yl)-1*H*-pyrazole-3-carboxamide (37).** Yield 87% (pale yellow solid), mp 122 °C. ^1H NMR ($CDCl_3$): δ 1.20–1.49 (m, 6H), 1.60–1.79 (m, 2H), 1.96–2.02 (m, 2H), 2.26 (s, 3H), 3.91–3.96 (m, 1H), 6.19–6.20 (m, 2H), 6.55–6.56 (m, 2H), 6.78–6.92 (m, 2H), 7.26–7.33 ppm (m, 1H). IR: ν 1660 cm^{-1}. MS *m/z*: 791 $[2M + Na]^+$ (100). Anal. ($C_{21}H_{22}F_2N_4O$ (384.42)) C, H, F, N.

***N*-Piperidin-1-yl 1-(2,4-Difluorophenyl)-5-(2,5-dimethyl-1*H*-pyrrol-1-yl)-4-methyl-1*H*-pyrazole-3-carboxamide (38).** Yield 60% (white solid), mp 175 °C. ^1H NMR ($CDCl_3$): δ 1.43–1.48 (m, 2H), 1.69–1.80 (m, 4H), 1.88 (s, 6H), 2.15 (s, 3H), 2.87 (t, J = 5.30 Hz, 4H), 5.78 (s, 2H), 6.83–6.92 (m, 2H), 7.06–7.23 (m, 1H), 7.65 ppm (broad s, 1H, disappeared on treatment with D_2O). IR: ν 1683 cm^{-1}. MS *m/z*: 414 $[M + 1]^+$ (100). Anal. ($C_{22}H_{25}F_2N_5O$ (413.46)) C, H, F, N.

***N*-3,4-Dichlorobenzyl 1-(2,4-difluorophenyl)-5-(2,5-dimethyl-1*H*-pyrrol-1-yl)-4-methyl-1*H*-pyrazole-3-carboxamide (39).** Yield 60% (white solid), mp 163 °C. ^1H NMR ($CDCl_3$): δ 1.89 (s, 6H), 2.18 (s, 3H), 4.56 (d, J = 6.23 Hz, 2H), 5.79 (s, 2H), 6.82–6.92 (m, 2H), 7.05–7.10 (m, 1H), 7.12–7.19 (m, 1H), 7.33–7.46 ppm (m, 2H). IR: ν 1674 cm^{-1}. MS *m/z*: 513 $[M + K]^+$ (100). Anal. ($C_{24}H_{20}Cl_2F_2N_4O$ (489.34)) C, H, Cl, F, N.

***N*-Cyclohexyl 1-(2,4-Difluorophenyl)-5-(2,5-dimethyl-1*H*-pyrrol-1-yl)-4-methyl-1*H*-pyrazole-3-carboxamide (40).** Yield 55% (yellow solid), mp 126 °C. ^1H NMR ($CDCl_3$): δ 1.19–1.46 (m, 6H), 1.69–1.78 (m, 2H), 1.88 (s, 6H), 1.95–2.04 (m, 2H), 2.15 (s, 3H), 3.93–3.97 (m, 1H), 5.78 (s, 2H), 6.83–6.92 (m, 2H), 7.08–7.19 ppm (m, 1H). IR: ν 1660 cm^{-1}. MS *m/z*: 413 $[M + 1]^+$ (100). Anal. ($C_{23}H_{26}F_2N_4O$ (412.48)) C, H, F, N.

***N*-Piperidin-1-yl 1-(2,4,6-Trichlorophenyl)-4-methyl-5-(1*H*-pyrrol-1-yl)-1*H*-pyrazole-3-carboxamide (41).** Yield 75% (pale yellow solid), mp 176–177 °C. ^1H NMR ($CDCl_3$): δ 1.38–1.47 (m, 2H), 1.65–1.79 (m, 4H), 2.25 (s, 3H), 2.85 (t, J = 5.28 Hz, 4H), 6.16–6.17 (m, 2H), 6.60–6.61 (m, 2H), 7.38 (s, 2H), 7.57 ppm (broad s, 1H, disappeared on treatment with D_2O). IR: ν 1684 cm^{-1}. MS *m/z*: 453 $[M + 1]^+$ (100). Anal. ($C_{20}H_{20}Cl_3N_5O$ (452.76)) C, H, Cl, N.

***N*-3,4-Dihlorobenzyl 1-(2,4,6-Trichlorophenyl)-4-methyl-5-(1*H*-pyrrol-1-yl)-1*H*-pyrazole-3-carboxamide (42).** Yield 68% (pale yellow solid), mp 72–74 °C. ^1H NMR (Acetone- d_6): δ 2.29 (s, 3H), 4.55 (d, J = 6.12 Hz, 2H), 6.17 (d, J = 1.87 Hz, 2H), 6.62 (d, J = 1.86 Hz, 2H), 7.17–7.23 (m, 1H), 7.37–7.44 ppm (m, 4H). IR: ν 1675 cm^{-1}. MS *m/z*: 551 $[M + Na]^+$ (100). Anal. ($C_{22}H_{15}Cl_5N_4O$ (528.65)) C, H, Cl, N.

***N*-Piperidin-1-yl 1-(2,4,6-Trichlorophenyl)-5-(2,5-dimethyl-1*H*-pyrrol-1-yl)-4-methyl-1*H*-pyrazole-3-carboxamide (43).** Yield 70% (pale yellow solid), mp 80–82 °C. ^1H NMR ($CDCl_3$): δ 1.40–1.45 (m, 2H), 1.71–1.79 (m, 4H), 1.94 (s, 6H), 2.11 (s, 3H), 2.87 (t, J = 5.32 Hz, 4H), 5.81 (s, 2H), 7.38 (s, 2H), 7.63 ppm (broad s, 1H, disappeared on treatment with D_2O). IR: ν 1683 cm^{-1}. MS *m/z*: 481 $[M + 1]^+$ (100). Anal. ($C_{22}H_{24}Cl_3N_5O$ (480.82)) C, H, Cl, N.

***N*-Cyclohexyl 1-(2,4,6-Trichlorophenyl)-5-(2,5-dimethyl-1*H*-pyrrol-1-yl)-4-methyl-1*H*-pyrazole-3-carboxamide (44).** Yield 78% (pale yellow solid), mp 130–131 °C. ^1H NMR ($CDCl_3$): δ 1.18–1.44 (m, 6H), 1.60–1.71 (m, 2H), 1.94 (s, 6H), 1.97–2.04 (m, 2H), 2.12 (s, 3H), 3.89–3.98 (m, 1H), 5.81 (s, 2H), 6.82 (broad s, 1H, disappeared on treatment with D_2O), 7.38 ppm (s, 2H). IR: ν 1662 cm^{-1}. MS *m/z*: 501 $[M + Na]^+$ (100). Anal. ($C_{23}H_{25}Cl_3N_4O$ (479.83)) C, H, Cl, N.

Potassium 1-Cyano-3-ethoxy-3-oxoprop-1-en-2-olate (45). Diethyl oxalate (4.30 g, 4.00 mL, 0.029 mol) was added to a solution of 18-crown-6 (0.63 g, 0.0024 mol) and potassium *tert*-butoxide (3.25 g, 0.029 mol) in anhydrous THF (27.26 mL) at 0 °C. The mixture was heated at 60 °C while anhydrous acetonitrile (1.19 g, 1.51 mL, 0.029 mol) was added dropwise, and then the reaction was stirred at 60 °C for 30 min. After cooling, the solid was filtered and washed with anhydrous diethyl ether to give **45** (3.96 g, yield 76%), mp 107–109 °C dec (lit.[50] mp 105 °C dec.).

Potassium 2-Cyano-4-ethoxy-4-oxobut-2-en-2-olate (46). Synthesized as **46** using propionitrile. Yield 84%, mp 113 °C dec. ^1H NMR (DMSO-d_6): δ 1.19 (t, J = 7.10 Hz, 3H), 1.51 (s, 3H), 4.02 ppm (q, J = 7.11 Hz, 2H). IR: ν 1708, 2174 cm^{-1}. Anal. ($C_7H_8KNO_3$ (193.24)) C, H, N.

Ethyl 2-Chloro-2-phenylhydrazonoacetate (47). A solution of aniline (10.24 g, 10.02 mL, 0.11 mol), 37% HCl (28 mL), ethanol (14 mL), and water (14 mL) was cooled at −5 °C, and then a solution of sodium nitrite (8.28 g, 0.12 mol) in water (38 mL) was added dropwise while the temperature was maintained below 5 °C. A cold solution of ethyl 2-chloroacetoacetate (18.10 g, 15.2 mL, 0.11 mol), sodium acetate trihydrate (22.45 g, 1.265 mol) in ethanol (270 mL), and water (30 mL) was added, and the reaction was stirred at −5 °C for 4 h. The reaction was quenched with water (4 L) and stirred overnight. The solid was collected and recrystallized from ethanol to furnish **47** (21.32 g, yield 85%), mp 77–79 °C (from ethanol; lit.[51] mp 78–79 °C). ^1H NMR ($CDCl_3$): δ 1.43 (t, J = 7.13 Hz, 3H), 4.41 (q, J = 7.12 Hz, 2H), 7.06 (t, J = 7.33 Hz, 1H), 7.25 (d, J = 7.64 Hz, 2H), 7.36 (t, J = 7.93 Hz, 2H), 8.36 ppm (broad s, 1H, disappeared on treatment with D_2O). IR: ν 1712, 3277 cm^{-1}. Anal. ($C_{10}H_{11}ClN_2O_2$ (226.66)) C, H, Cl, N.

Ethyl 2-Chloro-2-(4-chlorophenylhydrazono)acetate (48). Synthesized as **48** using 4-chloroaniline. Yield 97%, mp 144–145 °C (from ethanol; lit.[52] mp 144–145 °C). ^1H NMR (DMSO-d_6): δ 1.42 (t, J = 7.13 Hz, 3H), 4.40 (q, J = 7.13 Hz, 2H), 7.18 (d, J = 8.87 Hz, 2H), 7.30 (d, J = 8.98 Hz, 2H), 8.37 ppm (broad s, 1H, disappeared on treatment with D_2O). IR: ν 1706, 3264 cm^{-1}. Anal. ($C_{10}H_{10}Cl_2N_2O_7$ (261.10)) C, H, Cl, N.

Ethyl 5-Amino-4-methyl-1-phenyl-1*H*-pyrazole-3-carboxylate (50). HCl (37%, 0.35 mL) was added to a solution of phenylhydrazine (0.5 g, 0.45 mL, 0.0046 mol) and **46** (0.89 g, 0.0046 mol) in EtOH (10 mL). The reaction mixture was refluxed for 6 h, and after cooling, water was added and the reaction was extracted with ethyl acetate. The organic layer was washed with saturated sodium hydrogencarbonate solution and then with brine and dried. Removal of the solvent furnished a residue that was purified by silica gel column chromatography (ethyl acetate as eluent) to give **50** (0.63 g, yield 56%), mp 108–111 °C (from toluene). ^1H NMR (DMSO-d_6): δ 1.29 (t, J = 7.06 Hz, 3H), 2.10 (s, 3H), 4.25 (q, J = 6.99 Hz, 2H), 5.20 (broad s, 2H, disappeared on treatment with D_2O), 7.40–7.42 (m, 1H), 7.43–7.56 (m, 2H), 7.59–7.62 ppm (m, 2H). IR: ν 1708, 3329 cm^{-1}. Anal. ($C_{13}H_{15}N_3O_2$ (245.28)) C, H, N.

Ethyl 5-Amino-1-phenyl-1*H*-pyrazole-3-carboxylate (49). Synthesized as **50** using **45**. Yield 78%, mp 95–97 °C (from toluene). ^1H NMR (DMSO-d_6): δ 1.28 (t, J = 7.10 Hz, 3H), 4.25 (q, J = 7.11 Hz, 2H), 5.56 (broad s, 2H, disappeared on treatment with D_2O), 5.91 (s, 1H), 7.43 (t, J = 7.27 Hz, 1H), 7.54 (t, J = 7.75 Hz, 2H), 7.60 ppm (d, J = 7.34 Hz, 2H). IR: ν 1707, 3183, 3301, 3395 cm^{-1}. Anal. ($C_{12}H_{13}N_3O_2$ (231.25)) C, H, N.

Ethyl 5-Amino-4-cyano-1-phenyl-1*H*-pyrazole-3-carboxylate (51). Prepared as previously reported.[53] Yield 65%, mp 157–161 °C (from ethanol; lit.[50] mp 157 °C). ^1H NMR (DMSO-d_6): δ 1.29 (t, J = 7.09 Hz, 3H), 4.31 (q, J = 7.00 Hz, 2H), 6.40 (broad s, 2H, disappeared on treatment with D_2O), 7.49–7.59 ppm (m, 5H). IR: ν 1706, 2217, 3222, 3306 cm^{-1}. Anal. ($C_{13}H_{12}N_4O_2$ (256.26)) C, H, N.

Ethyl 5-Amino-1-(4-chlorophenyl)-1*H*-pyrazole-3-carboxylate (52). 4-Chlorophenylhydrazine hydrochloride (0.55 g, 0.0037 mol) was added to a suspension of **45** (0.50 g, 0.0028 mol) in EtOH (10 mL). The reaction mixture was refluxed for 2 h. After cooling, water was added and the precipitate was collected, washed with water, and recrystallized by ethanol to furnish **52** (0.51 g, yield 69%), mp

176–179 °C (from ethanol). ^{1}H NMR (DMSO-d_6): δ 1.29 (t, J = 7.10 Hz, 3H), 4.25 (q, J = 7.09 Hz, 2H), 5.64 (broad s, 2H, disappeared on treatment with D_2O), 5.91 (s, 1H), 7.58 (d, J = 7.30 Hz, 2H), 7.63 ppm (d, J = 8.94 Hz, 2H). IR: ν 1702, 3225, 3302, 3361 cm^{-1}. Anal. ($C_{12}H_{12}ClN_3O_2$ (265.70)) C, H, Cl, N.

Ethyl 5-Amino-1-(4-chlorophenyl)-4-methyl-1*H*-pyrazole-3-carboxylate (53). Synthesized as **52** using **46**. Yield 89%, mp 184–186 °C (from ethanol). ^{1}H NMR (DMSO-d_6): δ 1.29 (t, J = 7.06 Hz, 3H), 2.10 (s, 3H), 4.25 (q, J = 6.99 Hz, 2H), 5.28 (broad s, 2H, disappeared on treatment with D_2O), 7.57 (d, J = 8.57 Hz, 2H), 7.64 ppm (d, J = 8.81 Hz, 2H). IR: ν 1701, 3231, 3303, 3359 cm^{-1}. Anal. ($C_{13}H_{14}ClN_3O_2$ (279.72)) C, H, Cl, N.

Ethyl 5-Amino-1-(4-chlorophenyl)-4-cyano-1*H*-pyrazole-3-carboxylate (54). Synthesized as **51** using **48**. Yield 88%, mp 206–207 °C (from ethanol). ^{1}H NMR (DMSO-d_6): δ 1.29 (t, J = 7.11 Hz, 3H), 4.32 (q, J = 7.11 Hz, 2H), 7.00 (broad s, 2H, disappeared on treatment with D_2O), 7.57 (d, J = 8.84 Hz, 2H), 7.63 ppm (d, J = 8.86 Hz, 2H). IR: ν 1727, 2230, 3223, 3303, 3364 cm^{-1}. Anal. ($C_{13}H_{11}ClN_4O_2$ (290.71)) C, H, Cl, N.

Ethyl 5-Amino-1-(2,4-dichlorophenyl)-4-methyl-1*H*-pyrazole-3-carboxylate (55). Synthesized as **52** using 2,4-dichlorophenylhydrazine hydrochloride and **46**. Yield 47%, mp 179–181 °C (from ethanol). ^{1}H NMR ($CDCl_3$): δ 1.40 (t, J = 7.12 Hz, 3H), 2.20 (s, 3H), 3.47 (broad s, 2H, disappeared on treatment with D_2O), 4.40 (q, J = 7.11 Hz, 2H), 7.40 (dd, J = 2.06 and 8.45 Hz, 1H), 7.43 (d, J = 8.51 Hz, 1H), 7.56 ppm (d, J = 1.67 Hz, 1H). IR: ν 1709, 3183, 3383 cm^{-1}. Anal. ($C_{13}H_{13}Cl_2N_3O_2$ (314.17)) C, H, Cl, N.

Ethyl 5-Amino-1-(3,4-dichlorophenyl)-4-methyl-1*H*-pyrazole-3-carboxylate (56). Synthesized as **52** using 3,4-dichlorophenylhydrazine hydrochloride and **46**. Yield 62%, mp 92–96 °C (from ethanol). ^{1}H NMR (DMSO-d_6): δ 1.28 (t, J = 7.06 Hz, 3H), 2.09 (s, 3H), 4.25 (q, J = 7.05 Hz, 2H), 5.39 (broad s, 2H, disappeared on treatment with D_2O), 7.64 (dd, J = 2.04 and 8.45 Hz, 1H), 7.77 (d, J = 8.75 Hz, 1H), 7.89 ppm (d, J = 2.07 Hz, 1H). IR: ν 1702, 3361 cm^{-1}. Anal. ($C_{13}H_{13}Cl_2N_3O_2$ (314.17)) C, H, Cl, N.

Ethyl 5-Amino-1-(2,4-difluorophenyl)-4-methyl-1*H*-pyrazole-3-carboxylate (57). Synthesized as **52** using 2,4-difluorophenylhydrazine hydrochloride and **46**. Yield 65%, mp 92–94 °C (from chloroform). ^{1}H NMR ($CDCl_3$): δ 1.34 (t, J = 7.18 Hz, 3H), 2.13 (s, 3H), 4.31 (q, J = 7.05 Hz, 2H), 4.76 (broad s, 2H, disappeared on treatment with D_2O), 6.84–6.99 (m, 2H), 7.07–7.19 ppm (m, 1H). MS m/z: 304 $[M + Na]^+$ (100). Anal. ($C_{13}H_{13}F_2N_3O_2$ (281.26)) C, H, F, N.

Ethyl 5-Amino-4-methyl-1-(2,4,6-trichlorophenyl)-1*H*-pyrazole-3-carboxylate (58). Synthesized as **50** using 2,4,6-trichlorophenylhydrazine. Yield 40%, mp 209–211 °C (from ethanol). ^{1}H NMR ($CDCl_3$): δ 1.39 (t, J = 7.12 Hz, 3H), 2.23 (s, 3H), 3.35 (broad s, 2H, disappeared on treatment with D_2O), 4.40 (q, J = 7.12 Hz, 2H), 7.48 ppm (s, 2H). IR: ν 1702, 3329, 3420 cm^{-1}. Anal. ($C_{13}H_{12}Cl_3N_3O_2$ (348.61)). C, H, Cl, N.

Synthesis of Pyrrole Derivatives 59–65, 67, 69, and 71. General Procedure. Example: Ethyl 1-(4-Chlorophenyl)-4-cyano-5-(1*H*-pyrrol-1-yl)-1*H*-pyrazole-3-carboxylate (64). 2,5-Dimethoxytetrahydrofuran (10.97 g, 10.75 mL, 0.083 mol) was added to a solution of **54** (22.97 g, 0.079 mol) in glacial acetic acid (561 mL). The reaction was refluxed for 1 h. After cooling, water was added, and the mixture was concentrated to a small volume and extracted with saturated ethyl acetate. The organic layer was washed with saturated sodium hydrogencarbonate solution and then with brine and dried. Removal of the solvent gave a residue, which was purified by silica gel column chromatography (chloroform as eluent) to furnish **64** (18.80 g, yield 70%), mp 149–152 °C (from ethanol). ^{1}H NMR (DMSO-d_6): δ 1.35 (t, J = 7.08 Hz, 3H), 4.43 (q, J = 7.06 Hz, 2H), 6.33 (s, 2H), 6.99 (s, 2H), 7.31 (d, J = 8.80 Hz, 2H), 7.58 ppm (d, J = 8.82 Hz, 2H). IR: ν 1702, 2219 cm^{-1}. Anal. ($C_{17}H_{13}ClN_4O_2$ (340.76)) C, H, Cl, N.

Ethyl 1-Phenyl-5-(1*H*-pyrrol-1-yl)-1*H*-pyrazole-3-carboxylate (59). Synthesized as **64** using **49**. Yield 82%, mp 53–55 °C (from cyclohexane). ^{1}H NMR (DMSO-d_6): δ 1.30 (t, J = 7.09 Hz, 3H), 4.33 (q, J = 7.09 Hz, 2H), 6.19 (s, 2H), 6.84 (s, 2H), 7.06 (s, 1H), 7.19–7.22 (m, 2H), 7.37–7.43 ppm (m, 3H). IR: ν 1717 cm^{-1}. Anal. ($C_{16}H_{15}N_3O_2$ (281.31)) C, H, N.

Ethyl 4-Methyl-1-phenyl-5-(1*H*-pyrrol-1-yl)-1*H*-pyrazole-3-carboxylate (60). Synthesized as **64** using **50**. Yield 77%, mp 117–120 °C (from cyclohexane). ^{1}H NMR (DMSO-d_6): δ 1.30 (t, J = 7.09 Hz, 3H), 2.10 (s, 3H), 4.33 (q, J = 7.07 Hz, 2H), 6.24 (s, 2H), 6.86 (s, 2H), 7.14–7.16 (m, 2H), 7.34–7.40 ppm (m, 3H). IR: ν 1723 cm^{-1}. Anal. ($C_{17}H_{17}N_3O_2$ (295.34)) C, H, N.

Ethyl 4-Cyano-1-phenyl-5-(1*H*-pyrrol-1-yl)-1*H*-pyrazole-3-carboxylate (61). Synthesized as **64** using **51**. Yield 71%, mp 190–194 °C (from etanol). ^{1}H NMR (DMSO-d_6): δ 1.35 (t, J = 7.10 Hz, 3H), 4.43 (q, J = 7.09 Hz, 2H), 6.31 (s, 2H), 6.97 (s, 2H), 7.29–7.32 (m, 2H), 7.46–7.50 ppm (m, 3H). IR: ν 1719, 2242 cm^{-1}. Anal. ($C_{17}H_{14}N_4O_2$ (306.32)) C, H, N.

Ethyl 1-(4-Chlorophenyl)-5-(1*H*-pyrrol-1-yl)-1*H*-pyrazole-3-carboxylate (62). Synthesized as **64** using **52**. Yield 77%, yellow oil. ^{1}H NMR (DMSO-d_6): δ 1.33 (t, J = 7.10 Hz, 3H), 4.35 (q, J = 7.10 Hz, 2H), 6.24 (s, 2H), 6.89 (s, 2H), 7.10 (s, 1H), 7.22 (d, J = 8.77 Hz, 2H), 7.52 ppm (d, J = 8.78 Hz, 2H). IR: ν 1719 cm^{-1}. Anal. ($C_{16}H_{14}ClN_3O_2$ (315.75)) C, H, Cl, N.

Ethyl 1-(4-Chlorophenyl)-4-methyl-5-(1*H*-pyrrol-1-yl)-1*H*-pyrazole-3-carboxylate (63). Synthesized as **64** using **53**. Yield 80%, mp 79–82 °C (from ethanol). ^{1}H NMR (DMSO-d_6): δ 1.34 (t, J = 7.09 Hz, 3H), 2.12 (s, 3H), 4.35 (q, J = 7.10 Hz, 2H), 6.28 (s, 2H), 6.91 (s, 2H), 7.15 (d, J = 8.19 Hz, 2H), 7.48 ppm (d, J = 8.85 Hz, 2H). IR: ν 1716 cm^{-1}. Anal. ($C_{17}H_{16}ClN_3O_2$ (329.78)) C, H, Cl, N.

Ethyl 1-(2,4-Dichlorophenyl)-4-methyl-5-(1*H*-pyrrol-1-yl)-1*H*-pyrazole-3-carboxylate (65). Synthesized as **64** using **55**. Yield 91%, mp 179–181 °C (from ethanol). ^{1}H NMR ($CDCl_3$): δ 1.44 (t, J = 7.13 Hz, 3H), 2.28 (s, 3H), 4.47 (q, J = 7.13 Hz, 2H), 6.22 (s, 2H), 6.59 (s, 2H), 7.27–7.29 (m, 2H), 7.44–7.45 ppm (m, 1H). IR: ν 1716 cm^{-1}. Anal. ($C_{17}H_{15}Cl_2N_3O_2$ (364.23)) C, H, Cl, N.

Ethyl 1-(3,4-Dichlorophenyl)-4-methyl-5-(1*H*-pyrrol-1-yl)-1*H*-pyrazole-3-carboxylate (67). Synthesized as **64** using **56**. Yield 61%, mp 114–115 °C (from ethanol). ^{1}H NMR ($CDCl_3$): δ 1.46 (t, J = 7.12 Hz, 3H), 2.24 (s, 3H), 4.49 (q, J = 7.34 Hz, 2H), 6.39 (s, 2H), 6.65 (s, 2H), 6.84 (dd, J = 2.52 and 8.73 Hz, 1H), 7.33 (d, J = 2.34 Hz, 1H), 7.35 ppm (d, J = 8.72 Hz, 1H). IR: ν 1721 cm^{-1}. Anal. ($C_{17}H_{15}Cl_2N_3O_2$ (364.23)) C, H, Cl, N.

Ethyl 1-(2,4-Difluorophenyl)-4-methyl-5-(1*H*-pyrrol-1-yl)-1*H*-pyrazole-3-carboxylate (69). Synthesized as **64** using **57**. Yield 60%, mp 80–84 °C. ^{1}H NMR ($CDCl_3$): δ 1.40 (t, J = 7.27 Hz, 3H), 2.22 (s, 3H), 4.43 (q, J = 7.07 Hz, 2H), 6.19 (s, 2H), 6.56 (s, 2H), 6.80–6.91 (m, 2H), 7.27–7.39 ppm (m, 1H). IR: ν 1713 cm^{-1}. MS m/z: 354 $[M + Na]^+$ (100). Anal. ($C_{17}H_{15}F_2N_3O_2$ (331.32)) C, H, F, N.

Ethyl 4-Methyl-5-(1*H*-pyrrol-1-yl)-1-(2,4,6-trichlorophenyl)-1*H*-pyrazole-3-carboxylate (71). Synthesized as **64** using **58**. Yield 96%, brown oil. ^{1}H NMR ($CDCl_3$): δ 1.43 (t, J = 7.12 Hz, 3H), 2.25 (s, 3H), 4.40 (q, J = 7.14 Hz, 2H), 6.21 (s, 2H), 6.66 (s, 2H), 7.38 ppm (s, 2H). IR: ν 1711 cm^{-1}. Anal. ($C_{17}H_{14}Cl_3N_3O_2$ (398.67)) C, H, Cl, N.

Synthesis of Dimethylpyrrole Derivatives 66, 68, 70, and 72. General Procedure. Example: Ethyl 1-(3,4-Dichlorophenyl)-5-(2,5-dimethyl-1*H*-pyrrol-1-yl)-4-methyl-1*H*-pyrazole-3-carboxylate (68). A solution of **57** (2.01 g, 0.0064 mol) and acetonylacetone (0.80 g, 0.81 mL, 0.007 mol) in glacial acetic acid (15 mL) was refluxed for 1.5 h. After cooling, water was added and the reaction mixture was extracted with ethyl acetate. The organic layer was washed with saturated sodium hydrogencarbonate solution and then with brine and dried. Evaporation of the solvent gave a residue that was purified by silica gel column chromatography (chloroform as eluent) to furnish **68** (1.65 g, yield 65%), mp 74–78 °C (from ethanol). ^{1}H NMR ($CDCl_3$): δ 1.48 (t, J = 7.13 Hz, 3H), 1.88 (s, 6H), 2.19 (s, 3H), 4.50 (q, J = 7.12 Hz, 2H), 5.99 (s, 2H), 6.74 (dd, J = 2.56 and 8.81 Hz, 1H), 7.30 (d, J = 2.50 Hz, 1H), 7.35 ppm (d, J = 8.82 Hz, 1H). IR: ν 1717 cm^{-1}. Anal. ($C_{19}H_{19}Cl_2N_3O_2$ (392.28)) C, H, Cl, N.

Ethyl 1-(2,4-Dichlorophenyl)-5-(2,5-dimethyl-1*H*-pyrrol-1-yl)-4-methyl-1*H*-pyrazole-3-carboxylate (66). Synthesized as **68** using **55**. Yield 90%, yellow oil. ^{1}H NMR (DMSO-d_6): δ 1.33 (t, J = 7.10 Hz, 3H), 1.92 (s, 6H), 2.03 (s, 3H), 4.34 (q, J = 7.10 Hz, 2H), 5.79 (s, 2H), 7.26 (d, J = 8.58 Hz, 1H), 7.51 (dd, J = 2.33 and 8.57 Hz, 1H), 7.90 ppm (d, J = 2.29 Hz, 1H). IR: ν 1716 cm^{-1}. Anal. ($C_{19}H_{19}Cl_2N_3O_2$ (392.28)) C, H, Cl, N.

Ethyl 1-(2,4-Difluorophenyl)-5-(2,5-dimethyl-1*H*-pyrrol-1-yl)-4-methyl-1*H*-pyrazole-3-carboxylate (70). Synthesized as **68** using **57**. Yield 71%, mp 98–102 °C. ^{1}H NMR ($CDCl_3$): δ 1.41 (t, J = 6.98 Hz, 3H), 1.88 (s, 6H), 2.11 (s, 3H), 4.44 (q, J = 7.13 Hz, 2H), 5.78 (s, 2H), 6.80–6.88 (m, 2H), 7.15–7.26 ppm (m, 1H). IR ν 1714 cm^{-1}. MS m/z: 382 [M + Na]$^+$ (100). Anal. ($C_{19}H_{19}F_2N_3O_2$ (359.37)) C, H, F, N.

Ethyl 5-(2,5-Dimethyl-1*H*-pyrrol-1-yl)-4-methyl-1-(2,4,6-trichlorophenyl)-1*H*-pyrazole-3-carboxylate (72). Synthesized as **68** using **58**. Yield 87%, mp 109–112 °C (from ethanol). ^{1}H NMR ($CDCl_3$): δ 1.43 (t, J = 7.12 Hz, 3H), 1.98 (s, 6H), 2.10 (s, 3H), 4.47 (q, J = 7.12 Hz, 2H), 5.84 (s, 2H), 7.38 ppm (s, 2H). IR: ν 1712 cm^{-1}. Anal. ($C_{19}H_{18}Cl_3N_3O_2$ (426.72)) C, H, Cl, N.

Synthesis of Carboxylic Acids 73–86. General Procedure. Example: 1-(4-Chlorophenyl)-4-cyano-5-(1*H*-pyrrol-1-yl)-1*H*-pyrazole-3-carboxylic Acid (78). Lithium hydroxide monohydrate (0.15 g, 0.0036 mol) was added to a solution of **64** (0.40 g, 0.0018 mol) in THF (13 mL) and H_2O (8.6 mL). The reaction was stirred at room temperature overnight. The mixture was acidified with 1 N HCl to pH 2 and extracted with ethyl acetate. The organic layer was washed with brine and dried. After removal of the solvent, the residue was crystallized from ethanol to give **78** (0.36 g, yield 97%), mp 97–101 °C (from ethanol). ^{1}H NMR (DMSO-d_6): δ 6.32 (s, 2H), 6.98 (s, 2H), 7.30 (d, J = 8.64 Hz, 2H), 7.57 (d, J = 8.56 Hz, 2H), 13.32 ppm (broad s, 1H, disappeared on treatment with D_2O). IR: ν 1710, 2242 cm^{-1}. Anal. ($C_{15}H_9ClN_4O_2$ (312.71)) C, H, Cl, N.

1-Phenyl-5-(1*H*-pyrrol-1-yl)-1*H*-pyrazole-3-carboxylic Acid (73). Synthesized as **78** using **59**. Yield 83%, mp 218–221 °C (from ethanol). ^{1}H NMR (DMSO-d_6): δ 6.20 (s, 2H), 6.85 (s, 2H), 7.01 (s, 1H), 7.19–7.22 (m, 2H), 7.41–7.43 (m, 3H), 12.99 ppm (broad s, 1H, disappeared on treatment with D_2O). IR: ν 1686 cm^{-1}. Anal. ($C_{14}H_{11}N_3O_2$ (253.26)) C, H, N.

4-Methyl-1-phenyl-5-(1*H*-pyrrol-1-yl)-1*H*-pyrazole-3-carboxylic Acid (74). Synthesized as **78** using **60**. Yield 96%, mp 195–197 °C (from ethanol). ^{1}H NMR (DMSO-d_6): δ 2.08 (s, 3H), 6.24 (s, 2H), 6.87 (s, 2H), 7.12–7.16 (m, 2H), 7.34–7.41 (m, 3H), 13.18 ppm (broad s, 1H, disappeared on treatment with D_2O). IR: ν 1690 cm^{-1}. Anal. ($C_{15}H_{13}N_3O_2$ (263.28)) C, H, N.

4-Cyano-1-phenyl-5-(1*H*-pyrrol-1-yl)-1*H*-pyrazole-3-carboxylic Acid (75). Synthesized as **78** using **61**. Yield 97%, mp 226–227 °C (from ethanol). ^{1}H NMR (DMSO-d_6): δ 6.30 (s, 2H), 6.97 (s, 2H), 7.28–7.30 (m, 2H), 7.45–7.49 (m, 3H) 12.98 ppm (broad s, 1H, disappeared on treatment with D_2O). IR: ν 2238, 1709 cm^{-1}. Anal. ($C_{15}H_{10}N_4O_2$ (278.27)) C, H, N.

1-(4-Chlorophenyl)-5-(1*H*-pyrrol-1-yl)-1*H*-pyrazole-3-carboxylic Acid (76). Synthesized as **78** using **62**. Yield 94%, mp 153–155 °C (from ethanol). ^{1}H NMR (DMSO-d_6): δ 6.24 (s, 2H), 6.89 (s, 2H), 7.04 (s, 1H), 7.21 (d, J = 8.78 Hz, 2H), 7.51 (d, J = 8.79 Hz, 2H), 13.15 ppm (broad s, 1H, disappeared on treatment with D_2O). IR: ν 1709, 2238 cm^{-1}. Anal. ($C_{14}H_{10}ClN_3O_2$ (287.70)) C, H, Cl, N.

1-(4-Chlorophenyl)-4-methyl-5-(1*H*-pyrrol-1-yl)-1*H*-pyrazole-3-carboxylic Acid (77). Synthesized as **78** using **63**. Yield 96%, mp 202–206 °C (from ethanol). ^{1}H NMR (DMSO-d_6): δ 2.10 (s, 3H), 6.28 (s, 2H), 6.91 (s, 2H), 7.13 (d, J = 8.80 Hz, 2H), 7.47 (d, J = 8.76 Hz, 2H), 13.12 ppm (broad s, 1H, disappeared on treatment with D_2O). IR: ν 1684 cm^{-1}. Anal. ($C_{15}H_{12}ClN_3O_2$ (301.73)) C, H, Cl, N.

1-(2,4-Dichlorophenyl)-4-methyl-5-(1*H*-pyrrol-1-yl)-1*H*-pyrazole-3-carboxylic Acid (79). Synthesized as **78** using **65**. Yield 94%, mp 208–214 °C (from ethanol). ^{1}H NMR (DMSO-d_6): 2.11 (s, 3H), 6.13 (s, 2H), 6.78 (s, 2H), 7.55 (dd, J = 2.29 and 8.51 Hz, 1H), 7.70 (d, J = 8.53 Hz, 1H), 7.81 (d, J = 2.21 Hz, 1H), 13.41 ppm (broad s, 1H, disappeared on treatment with D_2O). IR: ν 1690 cm^{-1}. Anal. ($C_{15}H_{11}Cl_2N_3O_2$ (336.17)) C, H, Cl, N.

1-(2,4-Dichlorophenyl)-5-(2,5-dimethyl-1*H*-pyrrol-1-yl)-4-methyl-1*H*-pyrazole-3-carboxylic Acid (80). Synthesized as **78** using **66**. Yield 90%, mp 205–208 °C (from ethanol). ^{1}H NMR ($CDCl_3$): 1.96 (s, 6H), 2.18 (s, 3H), 5.83 (s, 2H), 6.94 (d, J = 8.59 Hz, 1H), 7.20 (dd, J = 2.25 and 8.57 Hz, 1H), 7.51 (d, J = 2.22 Hz, 1H), 13.23 ppm (broad s, 1H, disappeared on treatment with D_2O). IR: ν 1701 cm^{-1}. Anal. ($C_{17}H_{15}Cl_2N_3O_2$ (364.23)) C, H, Cl, N

1-(3,4-Dichlorophenyl)-4-methyl-5-(1*H*-pyrrol-1-yl)-1*H*-pyrazole-3-carboxylic Acid (81). Synthesized as **78** using **67**. Yield 99%, mp 217–220 °C (from ethanol). ^{1}H NMR (DMSO-d_6): 2.10 (s, 3H), 6.33 (s, 2H), 6.94 (s, 2H), 7.10 (dd, J = 2.51 and 8.75 Hz, 1H), 7.20 (d, J = 2.48 Hz, 1H), 7.68 (d, J = 8.76 Hz, 1H), 13.06 ppm (broad s, 1H, disappeared on treatment with D_2O). IR: ν 1690 cm^{-1}. Anal. ($C_{15}H_{11}Cl_2N_3O_2$ (336.17)) C, H, Cl, N.

1-(3,4-Dichlorophenyl)-5-(2,5-dimethyl-1*H*-pyrrol-1-yl)-4-methyl-1*H*-pyrazole-3-carboxylic Acid (82). Synthesized as **78** using **68**. Yield 99%, mp 178–172 °C (from ethanol). ^{1}H NMR (DMSO-d_6): 1.83 (s, 6H), 2.08 (s, 3H), 5.98 (s, 2H), 7.01–7.03 (m, 2H), 7.70 (d, J = 7.31 Hz, 1H), 13.35 ppm (broad s, 1H, disappeared on treatment with D_2O). IR: ν 1694 cm^{-1}. Anal. ($C_{17}H_{15}Cl_2N_3O_2$ (364.23)) C, H, Cl, N.

1-(2,4-Difluorophenyl)-4-methyl-5-(1*H*-pyrrol-1-yl)-1*H*-pyrazole-3-carboxylic Acid (83). Synthesized as **78** using **69**. Yield 90%, mp 168–170 °C (from chloroform). ^{1}H NMR ($CDCl_3$): δ 2.24 (s, 3H), 6.21 (s, 2H), 6.58 (s, 2H), 6.84–6.92 (m, 2H), 7.34–7.37 (m, 1H), 10.82 ppm (broad s, 1H, disappeared on treatment with D_2O). IR ν 1691 cm^{-1}. Anal. ($C_{15}H_{11}F_2N_3O_2$ (303.26)) C, H, F, N.

1-(2,4-Difluorophenyl)-5-(2,5-dimethyl-1*H*-pyrrol-1-yl)-4-methyl-1*H*-pyrazole-3-carboxylic Acid (84). Synthesized as **78** using **70**. Yield 90%, mp 168–170 °C (from chloroform). ^{1}H NMR ($CDCl_3$): δ 2.24 (s, 3H), 6.21 (s, 2H), 6.58 (s, 2H), 6.84–6.92 (m, 2H), 7.34–7.37 (m, 1H), 10.82 ppm (broad s, 1H, disappeared on treatment with D_2O). IR ν 1690 cm^{-1}. Anal. ($C_{15}H_{11}F_2N_3O_2$ (303.26)) C, H, F, N.

4-Methyl-5-(1*H*-pyrrol-1-yl)-1-(2,4,6-trichlorophenyl)-1*H*-pyrazole-3-carboxylic Acid (85). Synthesized as **78** using **71**. Yield 93%, mp 234–237 °C (from ethanol). ^{1}H NMR ($CDCl_3$): δ 2.27 (s, 3H), 6.23 (s, 2H), 6.67 (s, 2H), 7.39 (s, 2H), 13.25 ppm (broad s, 1H, disappeared on treatment with D_2O). IR: ν 1696 cm^{-1}. Anal. ($C_{15}H_{10}Cl_3N_3O_2$ (370.62)) C, H, Cl, N.

5-(2,5-Dimethyl-1*H*-pyrrol-1-yl)-4-methyl-1-(2,4,6-trichlorophenyl)-1*H*-pyrazole-3-carboxylic Acid (86). Synthesized as **78** using **72**. Yield 98%, mp 237–240 °C (from ethanol). ^{1}H NMR ($CDCl_3$): δ 1.99 (s, 6H), 2.14 (s, 3H), 5.86 (s, 2H), 7.40 (s, 2H), 13.12 ppm (broad s, 1H, disappeared on treatment with D_2O). IR: ν 1682, 1703 cm^{-1}. Anal. ($C_{17}H_{14}Cl_3N_3O_2$ (398.67)) C, H, Cl, N.

5-Amino-1-(4-chlorophenyl)-3-methyl-1*H*-pyrazole-4-carbonitrile (87). Prepared according to literature.[51] Yield 45%, mp 175–178 °C (lit.[52] mp 177–178 °C). ^{1}H NMR ($CDCl_3$): δ 2.31 (s, 3H), 4.58 (broad s, 2H, disappeared on treatment with D_2O), 7.44 (d, J = 9.07 Hz, 2H), 7.48 ppm (d, J = 9.00 Hz, 2H). IR: ν 2215, 3324, 3463 cm^{-1}. Anal. ($C_{11}H_9N_4$(232.67)) C, H, Cl, N.

1-(4-Chlorophenyl)-3-methyl-5-(1*H*-pyrrol-1-yl)-1*H*-pyrazole-4-carbonitrile (88). Synthesized as **64** using **87**. Yield 99%, mp 148–152 °C (from ethanol). ^{1}H NMR ($CDCl_3$): δ 2.49 (s, 3H), 6.37 (t, J = 2.19 Hz, 2H), 6.72 (t, J = 2.20 Hz, 2H), 7.08 (d, J = 9.01 Hz, 2H), 7.37 ppm (d, J = 9.01 Hz, 2H). IR: ν 2232 cm^{-1}. Anal. ($C_{15}H_{11}ClN_4$(282.73)) C, H, Cl, N.

1-(4-Chlorophenyl)-3-methyl-5-(1*H*-pyrrol-1-yl)-1*H*-pyrazole-4-carboxylic Acid (89). A solution of **88** (0.20 g, 0.00071 mol), 3 N NaOH (1.2 mL), and ethylene glycol (21 mL) was refluxed for 24 h. After cooling, the reaction was quenched with water and made acidic with 6 N HCl until pH 2. The mixture was extracted with ethyl acetate. The organic layer was washed with brine and dried. Evaporation of the solvent furnished a residue that was purified by silica gel column chromatography (ethyl acetate as eluent) to give **89** (0.17 g, yield 79%), mp 236–240 °C (from ethanol). ^{1}H NMR (DMSO-d_6): δ 2.45 (s, 3H), 6.18 (t, J = 2.18 Hz, 2H), 6.85 (d, J

= 2.18 Hz, 2H), 7.05 (d, J = 9.03 Hz, 2H), 7.43 (d, J = 9.03 Hz, 2H), 12.56 ppm (broad s, 1H, disappeared on treatment with D_2O). IR: ν 1670 cm^{-1}. Anal. ($C_{15}H_{12}ClN_3O_2$ (301.73)) C, H, Cl, N.

CB_1 and CB_2 Receptor Binding Assays. For both receptor binding assays, the new compounds were tested as previously described.[39]

Cyclic AMP Assay. Cyclic AMP assays were performed on intact confluent N18TG2 cells plated in six-well dishes and stimulated for 10 min at 37 °C with 1 μM forskolin in 400 μL of serum-free Dulbecco's modified Eagle's medium containing 20 mM HEPES, 0.1 mg/mL BSA, and 0.1 mM 1-methyl-3-isobutylxanthine.[54] Cells were treated with vehicle (methanol, 0.1%), compounds (at various concentrations) or WIN-55,212 (100 nM). After incubation, 800 μL of ethanol was added, cells were extracted, and cyclic AMP was determined by means of a cyclic AMP assay kit (Amersham, U.K.), as advised by the manufacturer.

Computational Methods. Molecular modeling and graphics manipulations were performed using the INSIGHTII (InsightII Molecular Modeling Package, Accelrys Inc., San Diego, CA) and UCSF-CHIMERA software packages,[55] running on a Silicon Graphics Tezro R16000 workstation. Model building and geometry optimizations of compounds **1**, **26**, and **30** were accomplished with the CVFF force field,[56] available within INSIGHTII. Energy minimizations and MD simulations were realized by employing the AMBER 9 program,[57] selecting the parm99 force field.[58]

Residue Indexing. The convention used for the amino acid identifiers, according to the approach of Ballesteros and Weinstein,[59] facilitates comparison of aligned residues within the family of Group A GPCRs. To the most conserved residue in a given TM (TMX, where X is the TM number) is assigned the number X.50, and residues within a given TM are then indexed relative to the 50 position.

Construction of the hCB_1 Receptor Homology Model. The structural model of the hCB_1 was built using the recently reported 2.8 Å crystal structure of b-Rho[42] (PDB entry code 1F88) as a structural template. Briefly, the hCB_1 sequence was retrieved from the SWISS-PROT database[60] and aligned with the sequence of b-Rho using CLUSTALW software[61] with the following settings: matrix, Blosum series; gap opening penalty, 10; gap extension penalty, 0.05. Afterward, we checked and, where necessary, manually corrected this alignment to reflect the known alignment features of class A GPCRs, such as the highly conserved positions and gap-free transmembrane regions. The final alignment was in good agreement with those previously published and consistent with literature.[62,63] Extension of each helix was contemplated by taking into account the experimental length of the b-Rho helices and the secondary structure prediction of hCB_1 obtained with the PSIPRED software,[64] as well as the sequence conservation in the possible extensions of the helices. Following Salo's suggestion,[62] we omitted the highly conserved proline residue P5.50(215) (Ballesteros−Weinstein's nomenclature[59]) of rhodopsin (which provides the main anchoring).

Individual TM helical segments were built as ideal helices (using Φ and φ angles of −63.0° and −41.6°, respectively) with side chains placed in prevalent rotamers and representative proline kink geometries. Each model helix was capped with an acetyl group at the *N*-terminus and an *N*-methyl group at the *C*-terminus. These structures were then grouped by adding one at a time until a helical bundle (TM region), matching the overall characteristics of the crystallographic structure of b-Rho, had been obtained. The relative orientations and interactions between the helices were adjusted on the basis of incorporated structural inferences from available experimental data, such as mutation and ligand binding studies,[65–67] cysteine scanning data,[68,69] and site-directed mutation experiments.[70–72]

We only modeled receptor TM domains, because the exact conformation of the extracellular loops (ELs) is not computable without an experimental receptor structure. In addition, the EL2 of b-Rho crystal structure[42] differs from that of CB_1 receptor (it is arranged to cover the ligand binding site). Besides different lengths of the loop, the CB receptors lack the conserved disulfide bridge between TM3 and EL2. As a result, the binding cleft around TM3-6 is likely to be different: EL2 occupies less volume in the upper part of the binding pocket in CB receptors than in b-Rho.[45]

Biophysical and mutation studies demonstrated that the inactive state of the CB_1 receptor is stabilized by two salt bridges. The first one is established between R3.50(214) and D6.30(338) at the intracellular side and keeps the intracellular ends of TM3 and TM6 close, constraining the receptor in the inactive state.[73,74] Upon activation, this salt bridge is broken with concomitant relaxation and rotation of TM6 relative to TM3.[75–77] The second salt bridge is formed between the extracellular K3.28(192) and D6.58(366). This bond might position an inactive state of K3.28(192) for ligand interaction rather than stabilize the receptor inactive conformation; this is well-demonstrated by the same level of constitutive activity exhibited by wild type (WT) CB_1 receptor and the CB1 K3.28(192)A mutant.[78] Therefore, the absence of the K3.28(192)/D6.58(366) salt bridge does not lead to greater ease of activation. Based on this evidence, receptor construction harmonic distance constraints were added between R3.50(214) and D6.30(338) and between K3.28(192) and D6.58(366).

After all connections were made, the whole structure was energy-minimized using the SANDER module of the AMBER suite of programs until the rmsd value of the conjugate gradient was 0.001 kcal/mol per Å. To avoid spurious changes in the general fold and helix packing due to some still unfavorable electrostatic interactions or steric clashes, an energy penalty force constant of 10 kcal/Å^2/mol on the protein backbone atoms was applied throughout these calculations. For the conformational refinement of the hCB_1, the minimized structure was then used as the starting point for subsequent 500 ps of MD simulation, during which the positional constraints on the protein backbone atoms were gradually released from 10 to 0.1 kcal/Å^2/mol. The options of MD at 300 K with 0.2 ps coupling constant were: time step of 1 fs; update every 25 fs. The lengths of bonds with hydrogen atoms were constrained according to the SHAKE algorithm.[79]

The average structure from the last 100 ps trajectory of MD was reminimized with backbone constraints in the secondary structure until a rms of 0.005 kcal/Å·mol was reached. The stereochemical quality of the resulting protein structures was evaluated by inspection of the Φ/φ Ramachandran plot obtained from PROCHECK analysis.[80,81] High quality protein models show >90% of the residues within the most favored regions of the Ramachandran plots. Analyzing hCB_1 model structure, 94% of the residues were within that region, and only six amino acids occupied disallowed regions, all far away from the binding site (Figure 5). The rms deviations between backbone atoms in all helices were compared to the X-ray structure of rhodopsin as a template. Figure 1S, Supporting Information, shows the final hCB_1 model compared with the b-Rho crystal structure. As expected, deviations from the ideal α-helical structure were located in the respective TM regions of both the receptors. The MD snapshots were obtained through the PTRAJ module of AMBER.

Docking Simulations. Docking of compounds **1**, **26**, and **30** to the energy-minimized hCB_1 receptor model was carried out using GOLD 3.1 version,[43,44] a genetic algorithm-based software, selecting GOLDScore as a fitness function. GOLDScore is made up of four components that account for protein–ligand binding energy: protein–ligand hydrogen bond energy (external H-bond), protein–ligand van der Waals energy (external vdw), ligand internal vdw energy (internal vdw), and ligand torsional strain energy (internal torsion). Parameters used in the fitness function (H-bond energies, atom radii and polarizabilities, torsion potentials, H-bond directionalities, and so forth) are taken from the GOLD parameter file. The fitness score is taken as the negative of the sum of the energy terms, so larger fitness scores indicated better bindings. The fitness function has been optimized for the prediction of ligand binding positions rather than the prediction of binding affinities, although some correlation with the latter can also be found.[82] The protein input file may be the entire protein structure or a part of it comprising only the residues that are in the region of the ligand binding site. In the present study, GOLD was allowed to calculate

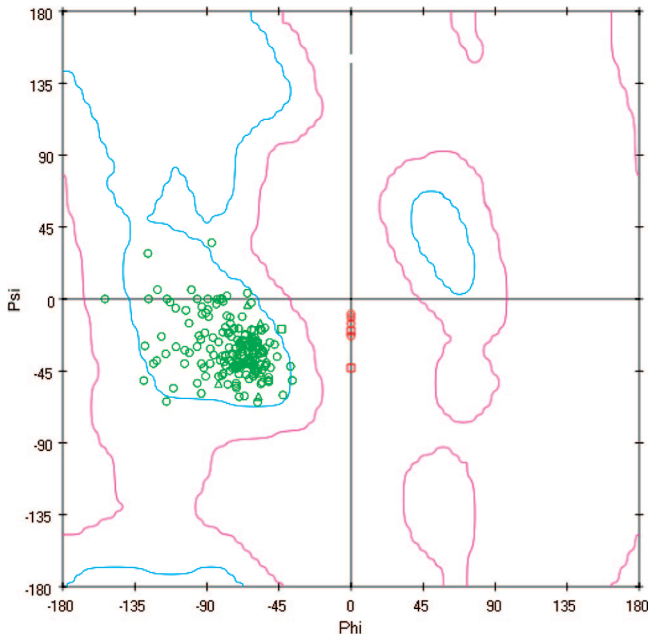

Figure 5. Ramachandran plot of the hCB_1 receptor model. The most favoured and the additional allowed regions are defined by cyan and magenta lines, respectively. The disallowed regions are indicated as white fields.

interaction energies within a sphere of an 18 Å radius centered on the side-chain nitrogen of K3.28(192).

The structures of the ligands **1**, **26**, and **30** were constructed using standard bond lengths and bond angles of the INSIGHTII fragment library. A total of 50 independent docking runs were performed for each docking experiment, using standard default settings with a population size of 100, a maximum number of 100000 operations, and a mutation and crossover rate of 95. The best-generated 20 solutions of each ligand were ranked according to their fitness scores calculated by the GOLDScore function.

MD Simulations. General AMBER force field (GAFF) parameters were assigned to ligands, while the partial charges were calculated using the AM1-BCC method, as implemented in the ANTECHAMBER suite of AMBER. The initial **1**/hCB_1, **26**/hCB_1, and **30**/hCB_1 complexes were energy-minimized for 10500 steps using combined steepest descent and conjugate gradient methods until a convergence value of 0.001 kcal/Å·mol. Upon minimization, an energy penalty force constant of 5 kcal/$Å^2$/mol on the protein backbone atoms was applied. The geometry-optimized complexes were then used as the starting point for subsequent 400 ps MD simulation, during which the positional constraints on the protein backbone were gradually reduced from 5 to 0.1 kcal/$Å^2$/mol. For the MD simulations were used the following: time step of 1 fs; pairlist update every 25 fs. The temperature was maintained at 300 K using the Berendsen algorithm[83] with a 0.2 ps coupling constant. The SHAKE method[79] was applied to constrain all of the covalent bonds involving hydrogen atoms. An average structure was calculated from the last 100 ps trajectory and energy-minimized using the steepest descent and conjugate gradient methods as specified above. The PTRAJ module of AMBER was used to check rmsd and interatomic distances. The H-bond criterion was a maximum donor–acceptor distance of 3.5 Å and a minimum donor−proton−acceptor angle of 120°.

Acknowledgment. Authors from the University of Siena wish to thank the Ministero dell'Università e della Ricerca (PRIN 2006 - Prot. n 2006030948_002) for financial support. Authors also thank Mr. Marco Allarà for technical assistance.

Supporting Information Available: Additional chemical and biological information. This material is available free of charge via Internet at http://pubs.acs.org.

References

(1) Di Marzo, V.; Bifulco, M.; De Petrocellis, L. The endocannabinoid system and its therapeutic exploitation. *Nat. Rev. Drug Discovery* **2004**, *3*, 771–784.

(2) Piomelli, D. The endocannabinoid system: A drug discovery perspective. *Curr. Opin. Invest. Drugs* **2005**, *6*, 672–679.

(3) (a) Maione, S.; Starowicz, K.; Palazzo, E.; Rossi, F.; Di Marzo, V. The endocannabinoid and endovanilloid systems and their interactions in neuropathic pain. *Drug Dev. Res.* **2006**, *67*, 339–354. (b) Bifulco, M.; Laezza, C.; Gazzerro, P.; Pentimalli, F. Endocannabinoids as emerging suppressors of angiogenesis and tumor invasion. *Oncol. Rep.* **2007**, *17*, 813–816. (c) Matias, I.; Di Marzo, V. Endocannabinoids and the control of energy balance. *Trends Endocrinol. Metab.* **2007**, *18*, 27–37. (d) Woods, S. C. The endocannabinoid system: mechanisms behind metabolic homeostasis and imbalance. *Am. J. Med.* **2007**, *120*, S9–S17.

(4) (a) Di Marzo, V.; De Petrocellis, L. Plant, synthetic, and endogenous cannabinoids in medicine. *Ann. Rev. Med.* **2006**, *57*, 553–574. (b) Di Marzo, V. A brief history of cannabinoid and endocannabinoid pharmacology as inspired by the work of British scientists. *Trends Pharmacol. Sci.* **2006**, *27*, 134–140. (c) Lambert, D. M.; Fowler, C. J. The endocannabinoid system: Drug targets, lead compounds, and potential therapeutic applications. *J. Med. Chem.* **2005**, *48*, 5059–5087.

(5) (a) Goutopoulos, A.; Makriyannis, A. From cannabis to cannabinergics: New therapeutic opportunities. *Pharm. Ther.* **2002**, *95*, 103–117. (b) Bellocchio, L.; Mancini, G.; Vicennati, V.; Pasquali, R.; Pagotto, U. Cannabinoid receptors as therapeutic targets for obesity and metabolic diseases. *Curr. Opin. Pharm.* **2006**, *6*, 586–591. (c) Pavlopoulos, S.; Thakur, G. A.; Nikas, S. P.; Makriyannis, A. Cannabinoid receptors as therapeutic targets. *Curr. Pharm. Des.* **2006**, *12*, 1751–1769.

(6) Antel, J.; Gregory, P. C.; Nordheim, U. CB_1 cannabinoid receptor antagonists for treatment of obesity and prevention of comorbid metabolic disorders. *J. Med. Chem.* **2006**, *49*, 4008–4016.

(7) Brotchie, J. M. CB_1 cannabinoid receptor signaling in Parkinson's disease. *Curr. Opin. Pharmacol.* **2003**, *3*, 54–61.

(8) Muller-Vahl, K. R. Cannabinoids reduce symptoms of Tourette's syndrome. *Expert Opin. Pharmacother.* **2003**, *4*, 1717–1725.

(9) Lastres-Becker, I.; de Miguel, R.; De Petrocellis, L.; Makriyannis, A.; Di Marzo, V.; Fernandez-Ruiz, J. Compounds acting at the endocannabinoid and/or endovanilloid systems reduce hyperkinesia in a rat model of Huntington's disease. *J. Neurochem.* **2003**, *84*, 1097–1109.

(10) Calignano, A.; Katona, I.; Desarnaud, F.; Giuffrida, A.; La Rana, G.; Mackie, K.; Freund, T. F.; Piomelli, D. Bidirectional control of airway responsiveness by endogenous cannabinoids. *Nature* **2000**, *408*, 96–101.

(11) Song, Z. H.; Slowey, C. A. Involvement of cannabinoid receptors in the intraocular pressure-lowering effects of WIN55212–2. *J. Pharmacol. Exp. Ther.* **2000**, *292*, 136–139.

(12) Pinto, L.; Izzo, A. A.; Cascio, M. G.; Bisogno, T.; Hospodar-Scott, K.; Brown, D. R.; Mascolo, N.; Di Marzo, V.; Capasso, F. Endocannabinoids as physiological regulators of colonic propulsion in mice. *Gastroenterology* **2002**, *123*, 227–234.

(13) (a) Lange, J. H. M.; Kruse, C. G. Medicinal chemistry strategies to CB_1 cannabinoid receptor antagonists. *Drug Discovery Today* **2005**, *10*, 693–702. (b) Barth, F. CB_1 cannabinoid receptor antagonist. *Annu. Rep. Med. Chem.* **2005**, *40*, 103–118. (c) Muccioli, G. G.; Lambert, D. M. Latest advances in cannabinoid receptor antagonists and inverse agonists. *Exp. Opin. Ther. Pat.* **2006**, *16*, 1405–1423.

(14) Tucci, S. A.; Halford, J. C. G.; Harrold, J. A.; Kirkham, T. C. Therapeutic potential of targeting the endocannabinoids; implications for the treatment of obesity, metabolic syndrome, drug abuse and smoking cessation. *Curr. Med. Chem.* **2006**, *13*, 2669–2680.

(15) Malan, T. P., Jr.; Ibrahim, M. M.; Lai, J.; Vanderah, T. W.; Makriyannis, A.; Porreca, F. CB_2 cannabinoid receptor agonists: Pain relief without psychoactive effects. *Curr. Opin. Pharmacol.* **2003**, *3*, 62–67.

(16) Iwamura, H.; Suzuki, H.; Ueda, Y.; Kaya, T.; Inaba, T. In vitro and in vivo pharmacological characterization of JTE-907, a novel selective ligand for cannabinoid CB_2 receptor. *J. Pharmacol. Exp. Ther.* **2001**, *296*, 420–425.

(17) Ofek, O.; Karsak, M.; Leclerc, N.; Fogel, M.; Frenkel, B.; Wright, K.; Tam, J.; Attar-Namdar, M.; Kram, V.; Shohami, E.; Mechoulam, R.; Zimmer, A.; Bab, I. Peripheral cannabinoid receptor, CB_2, regulates bone mass. *Proc. Natl. Acad. Sci. U.S.A.* **2006**, *103*, 696–701.

(18) Sanchez, C.; de Ceballos, M. L.; del Pulgar, T. G.; Rueda, D.; Corbacho, C.; Velasco, G.; Galve-Roperh, I.; Huffman, J. W.; Ramon y Cajal, S.; Guzman, M. Inhibition of glioma growth in vivo by selective activation of the CB_2 cannabinoid receptor. *Cancer Res.* **2001**, *61*, 5784–5789.

(19) McKallip, R. J.; Lombard, C.; Fisher, M.; Martin, B. R.; Ryu, S.; Grant, S.; Nagarkatti, P. S.; Nagarkatti, M. Targeting CB_2 cannabinoid receptors as a novel therapy to treat malignant lymphoblastic disease. *Blood* **2002**, *100*, 627–634.
(20) Pertwee, R. G. Cannabinoids and multiple sclerosis. *Pharmacol. Ther.* **2002**, *95*, 165–174.
(21) (a) Rinaldi-Carmona, M.; Barth, F.; Héaulme, M.; Shire, D.; Calandra, B.; Congy, C.; Martinez, S.; Maruani, J.; Néliat, G.; Caput, D.; Ferrara, P.; Soubrié, P.; Brelière, J. C.; Le Fur, G. SR141716A, a potent and selective antagonist of the brain cannabinoid receptor. *FEBS Lett.* **1994**, *350*, 240–244. (b) Sorbera, L. A.; Castaner, J.; Silvestre, J. S. Rimonabant hydrochloride. *Drugs Future* **2005**, *30*, 128–137.
(22) Marketing authorization of European Medicines Agency (EMEA) valid throughout the European Union: 19 June 2006. European Public Assessment Report (EPAR). Acomplia. Protocol EMEA/H/C/666.
(23) Padwal, R. S.; Majumdar, S. R. Drug treatments for obesity: Orlistat, sibutramine, and rimonabant. *Lancet* **2007**, *369*, 71–77.
(24) Halford, J. C. G. Obesity drugs in clinical development. *Curr. Opin. Invest. Drugs* **2006**, *7*, 312–318.
(25) Gatley, S. J.; Lan, R.; Pyatt, B.; Gifford, A. N.; Vollow, N. D.; Makriyannis, A. Binding of the non-classical cannabinoid CP 55,940, and the diarylpyrazole AM251 to rodent brain cannabinoid receptors. *Life Sci.* **1997**, *61*, PL191–PL197.
(26) Lan, R.; Gatley, J.; Lu, Q.; Fan, P.; Fernando, S. R.; Volkow, N. D.; Pertwee, R.; Makriyannis, A. Design and synthesis of the CB_1 selective cannabinoid antagonist AM281: a potential human SPECT ligand. *AAPS Pharm. Sci.* **1999**, *1*, 1–7.
(27) Lange, J. H. M.; Coolen, H. K. A. C.; van Stuivenberg, H. H.; Dijksman, J. A. R.; Herremans, A. H. J.; Ronken, E.; Keizer, H. G.; Tipker, K.; McCreary, A. C.; Veerman, W.; Wals, H. C.; Stork, B.; Verveer, P. C.; den Hartog, A. P.; Natasja, M. J.; de Jong, N. M. J.; Adolfs, T. J. P.; Hoogendoorn, J.; Kruse, C. G. Synthesis, biological properties, and molecular modeling investigations of novel 3,4-diarylpyrazolines as potent and selective CB_1 cannabinoid receptor antagonists. *J. Med. Chem.* **2004**, *47*, 627–643.
(28) Rinaldi-Carmona, M.; Barth, F.; Millan, J.; Derocq, J. M.; Casellas, P.; Congy, C.; Oustric, D.; Sarran, M.; Bouaboula, M.; Calandra, B.; Portier, M.; Shire, D.; Breliere, J. C.; Le Fur, G. L. SR 144528, the first potent and selective antagonist of the CB_2 cannabinoid receptor. *J. Pharmacol. Exp. Ther.* **1998**, *284*, 644–650.
(29) Plummer, C. W.; Finke, P. E.; Mills, S. G.; Wang, J.; Tong, X.; Doss, G. A.; Fong, T. M.; Lao, J. Z.; Schaeffer, M.-T.; Chen, J.; Shen, C.-P.; Stribling, D. S.; Shearman, L. P.; Starck, A. M.; Van der Ploeg, L. H. T. Synthesis and activity of 4,5-diarylimidazoles as human CB_1 receptor inverse agonists. *Bioorg. Med. Chem. Lett.* **2005**, *15*, 1441–1446.
(30) Lange, J. H. M.; Van Stuivenberg, H. H.; Coolen, H. K. A. C.; Adolfs, T. J. P.; McCreary, A. C.; Keizer, H. G.; Wals, H. C.; Veerman, W.; Borst, A. J. M.; De Looff, W.; Verveer, P. C.; Kruse, C. G. Bioisosteric replacements of the pyrazole moiety of rimonabant: synthesis, biological properties, and molecular modeling investigations of thiazoles, triazoles, and imidazoles as potent and selective CB_1 cannabinoid receptor antagonists. *J. Med. Chem.* **2005**, *48*, 1823–1838.
(31) Bergren, A. I. K.; Bostrom S. J.; Cheng, L. ; Elebring. S. T.; Greasley, P.; Nagard, M.; Wilstermann, J. M; Terricabras, E. 1,5-Diarylpyrrole-3-carboxamide derivatives and their use as cannabinoid receptor modulators. Patent WO2004058249, 2004.
(32) Barth, F.; Martinez, S.; Rinaldi-Carmona, M. Terphenyl derivatives, preparation thereof, compositions containing same. Patent WO03084943, 2003.
(33) Meurer, L. C.; Finke, P. E.; Mills, S. G.; Walsh, T. F.; Toupence, R. B.; Goulet, M. T.; Wang, J.; Tong, X.; Fong, T. M.; Lao, J.; Schaeffer, M.-T.; Chen, J.; Shen, C.-P.; Stribling, D. S.; Shearman, L. P.; Starck, A. M.; Van der Ploeg, L. H. T. Synthesis and SAR of 5,6-diarylpyridines as human CB_1 inverse agonists. *Bioorg. Med. Chem. Lett.* **2005**, *15*, 645–651.
(34) Kopka, I. E.; Li, B.; Hagmann, W. K. Substituted pyrimidines. Patent WO2004029204, 2004.
(35) (a) For example, see: Silvestri, R.; La Regina, G.; De Martino, G.; Artico, A.; Befani, O.; Palumbo, M.; Agostinelli, E.; Turini, P. Simple, potent and selective pyrrole inhibitors of monoamine oxidase type A and type B. *J. Med. Chem.* **2003**, *46*, 917–920. (b) Silvestri, R.; Artico, M.; La Regina, G.; De Martino, G.; La Colla, M.; Loddo, R.; La Colla, P. Anti-HIV-1 activity of pyrryl aryl sulfone (PAS) derivatives. synthesis and SAR studies of novel esters and amides at the position 2 of the pyrrole nucleus. *Farmaco* **2004**, *59*, 201–210. (c) Silvestri, R.; Marfè, G.; Artico, M.; La Regina, G.; De Martino, G.; Lavecchia, A.; Novellino, E.; Morgante, E.; Di Stefano, C.; Catalano, G.; Filomeni, G.; Abruzzese, E.; Ciriolo, M. R.; Russo, M. A.; Amadori, S.; Cirilli, R.; La Torre, F.; Sinibaldi Salimei, P. Pyrrolo[1,2- *b*][1,2,5]benzothiadiazepines (PBTDs): A new class of agents endowed with high apoptotic activity in chronic myelogenous leukemia K562 cells and in cells from patients at onset and Imatinib-resistant. *J. Med. Chem.* **2006**, *49*, 5840–5844.
(36) Corelli, F.; Massa, S.; Stefancich, G.; Silvestri, R.; Artico, M.; Pantaleoni, G. C.; Palumbo, G.; Fanini, D.; Giorgi, R. Agenti antiinfiammatori non-steroidei. Nota V. Sintesi di acidi 1-aril-5-(1-pirril)pirazolil-4-acetici a potenziale attività antiinfiammatoria. *Farmaco* **1988**, *43*, 251–265.
(37) (a) Elming, N.; Clauson-Kaas, N. The preparation of Pyrroles from furans. *Acta Chem. Scand.* **1952**, *6*, 867–74. (b) Clauson-Kaas, N.; Tyle, Z. Preparation of *cis*- and *trans*-2,5-dimethoxy-2-(acetamidomethyl)-2,5-dihydrofuran, of *cis*- and *trans*-2,5-dimethoxy-2-(acetamidomethyl)-tetrahydrofuran, and of 1-phenyl-2-(acetamidomethyl)pyrrole. *Acta Chem. Scand.* **1952**, *6*, 667–670.
(38) Peet, N. P.; Kim, H.-O. Parallel solution-phase synthesis. *Drug Discovery Dev.* **2006**, *1*, 169–198.
(39) Brizzi, A.; Brizzi, V.; Cascio, M. G.; Bisogno, T.; Siriani, R.; Di Marzo, V. Design, synthesis, and binding studies of new potent ligands of cannabinoid receptors. *J. Med. Chem.* **2005**, *48*, 7343–7350.
(40) Cheng, Y.; Prusoff, W. H. Relationship between the inhibition constant (K1) and the concentration of inhibitor which causes 50% inhibition (I_{50}) of an enzymatic reaction. *Biochem. Pharmacol.* **1973**, *22*, 3099–3108.
(41) Meschler, J. P.; Kraichely, D. M.; Wilken, G. H.; Howlett, A. C. Inverse agonist properties of *N*-(piperidin-1-yl)-5-(4-chlorophenyl)-1-(2,4-dichlorophenyl)-4-methyl-1H-pyrazole-3-carboxamide HCl (SR141716A) and 1-(2-chlorophenyl)-4-cyano-5-(4-methoxyphenyl)-1H-pyrazole-3-carboxylic acid phenylamide (CP-272871) for the CB_1 cannabinoid receptor. *Biochem. Pharmacol.* **2000**, *60*, 1315–1323.
(42) Palczewski, K.; Kumasaka, T.; Hori, T.; Behnke, C. A.; Motoshima, H.; Fox, B. A.; Trong, I. L.; Teller, D. C.; Okada, T.; Stenkamp, R. E.; Yamamoto, M.; Miyano, M. Crystal structure of rhodopsin: a G protein-coupled receptor. *Science* **2000**, *289*, 739–745.
(43) *GOLD 3.1*; CCDC Software Limited: Cambridge, U.K., 2004.
(44) Jones, G.; Willett, P.; Glen, R. C.; Leach, A. R.; Taylor, R. Development and validation of a genetic algorithm for flexible docking. *J. Mol. Biol.* **1997**, *267*, 727–748.
(45) Hurst, D. P.; Lynch, D. L.; Barnett-Norris, J.; Hyatt, S. M.; Seltzman, H. H.; Zhong, M.; Song, Z. H.; Nie, J.; Lewis, D.; Reggio, P. H. *N*-(Piperidin-1-yl)-5-(4-chlorophenyl)-1-(2,4-dichlorophenyl)-4-methyl-1*H*-pyrazole-3-carboxamide (SR141716A) interaction with LYS3.28(192) is crucial for its inverse agonism at the cannabinoid CB1 receptor. *Mol. Pharmacol.* **2002**, *62*, 1274–1287.
(46) McAllister, S. D.; Rizvi, G.; Anavi-Goffer, S.; Hurst, D. P.; Barnett-Norris, J.; Lynch, D. L.; Reggio, P. H.; Abood, M. E. An aromatic microdomain at the cannabinoid CB_1 receptor constitutes an agonist/inverse agonist binding region. *J. Med. Chem.* **2003**, *46*, 5139–5152.
(47) Hurst, D.; Umejiego, U.; Lynch, D.; Seltzman, H.; Hyatt, S.; Roche, M.; McAllister, S.; Fleischer, D.; Kapur, A.; Abood, M.; Shi, S.; Jones, J.; Lewis, D.; Reggio, P. Biarylpyrazole inverse agonists at the cannabinoid CB_1 receptor: Importance of the C-3 carboxamide oxygen/lysine3.28(192) interaction. *J. Med. Chem.* **2006**, *49*, 5969–5987.
(48) Kapur, A.; Hurst, D. P.; Fleischer, D.; Whitnell, R.; Thakur, G. A.; Makriyannis, A.; Reggio, P. H.; Abood, M. E. Mutation studies of S7.39 and S2.60 in the human CB_1 cannabinoid receptor: Evidence for a serine induced bend in CB_1 transmembrane helix 7. *Mol. Pharmacol.* **2007**, *71*, 1512–1524.
(49) Shire, D.; Calandra, B.; Delpech, M.; Dumont, X.; Kaghad, M.; Le Fur, G.; Caput, D.; Ferrara, P. Structural features of the central cannabinoid CB_1 receptor involved in the binding of the specific CB_1 antagonist SR 141716A. *J. Biol. Chem.* **1996**, *271*, 6941–6946.
(50) Rzepecki, P.; Gallmeier, H.; Geib, N.; Cernovska, K.; Koenig, B.; Schrader, T. New heterocyclic β-sheet ligands with peptidic recognition elements. *J. Org. Chem.* **2004**, *69*, 5168–5178.
(51) The compound was reported but not characterized by: Anderson, W. K.; Jones, A. N. Synthesis and evaluation of furan, thiophene, and azole bis[(carbamoyloxy)methyl]derivatives as potential antineoplastic agents. *J. Med. Chem.* **1984**, *27*, 1559–1565.
(52) Abdehamid, A. O.; Parkanyi, C.; Shawali, A. S.; Abdalla, M. A. New heterocyclic syntheses from hydrazidoyl halides. Convenient syntheses of fused pyrimidines, pyridazines, and quinazolines. *J. Heterocycl. Chem.* **1984**, *21*, 1049–1054.
(53) Southwick, P. L.; Dhawan, B. Preparation of 4,6-diaminopyrazolo[3,4-*d*]pyrimidines with variations in substitution at the 1- and 3-positions. *J. Heterocycl. Chem.* **1975**, *12*, 1199–1205.
(54) Melck, D.; Rueda, D.; Galve-Roperh, I.; De Petrocellis, L.; Guzman, M.; Di Marzo, V. Involvement of the cAMP/protein kinase A pathway and of mitogen-activated protein kinase in the anti-proliferative effects of anandamide in human breast cancer cells. *FEBS Lett.* **1999**, *463*, 235–240.
(55) Huang, C. C.; Couch, G. S.; Pettersen, E. F.; Ferrin, T. E. Chimera: An extensible molecular modelling application constructed using standard components. *Pac. Symp. Biocomput.* **1996**; *724*, 1; http://www.cgl.ucsf.edu/chimera.

(56) Hagler, A. F.; Lifson, S.; Dauber, P. Consistent force field studies of intermolecular forces in hydrogen-bonded crystals. *J. Am. Chem. Soc.* **1979**, *101*, 5122–5130.
(57) Case, D. A.; Darden, T. A.; Cheatham, T. E., III; Simmerling, C. L.; Wang, J.; Duke, R. E.; Luo, R.; Merz, K. M.; Pearlman, D. A.; Crowley, M.; Walker, R. C.; Zhang, W.; Wang, B.; Hayik, S.; Roitberg, A.; Seabra, G.; Wong, K. F.; Paesani, F.; Wu, X.; Brozell, S.; Tsui, V.; Gohlke, H.; Yang, L.; Tan, C.; Mongan, J.; Hornak, V.; Cui, G.; Beroza, P.; Mathews, D. H.; Schafmeister, C.; Ross, W. S.; Kollman, P. A. *AMBER 9*; University of California, San Francisco, CA, 2006.
(58) Cornell, W. D.; Cieplak, P.; Bayly, C. I.; Gould, I. R.; Merz, K. M., Jr.; Ferguson, D. M.; Spellmeyer, D. C.; Fox, T.; Caldwell, J. W.; Kollman, P. A. A second generation force field for the simulation of proteins, nucleic acids, and organic molecules. *J. Am. Chem. Soc.* **1995**, *117*, 5179–5197.
(59) Ballesteros, J. A.; Weinstein, H. Integrated methods for modeling G-protein coupled receptors. *Methods Neurosci.* **1996**, *25*, 366–428.
(60) Bairoch, A.; Apweiler, R. The SWISS-PROT protein sequence database and its supplement TrEMBL in 2000. *Nucleic Acids Res.* **2000**, *28*, 45–48.
(61) Thompson, J. D.; Higgins, D. G.; Gibson, T. J. CLUSTAL W: Improving the sensitivity of progressive multiple sequence alignment through sequence weighting, position-specific gap penalties and weight matrix choice. *Nucleic Acids Res.* **1994**, *22*, 4673–4680.
(62) Salo, O. M.; Lahtela-Kakkonen, M.; Gynther, J.; Jarvinen, T.; Poso, A. Development of a 3D model for the human cannabinoid CB_1 receptor. *J. Med. Chem.* **2004**, *47*, 3048–3057.
(63) Tuccinardi, T.; Ferrarini, P. L.; Manera, C.; Ortore, G.; Saccomanni, G.; Martinelli, A. Cannabinoid CB_2/CB_1 selectivity. Receptor modeling and automated docking analysis. *J. Med. Chem.* **2006**, *49*, 984–994.
(64) McGuffin, L. J.; Bryson, K.; Jones, D. T. The PSIPRED protein structure prediction server. *Bioinformatics* **2000**, *16*, 404–405.
(65) Baldwin, J. M. Structure and function of receptors coupled to G proteins. *Curr. Opin. Cell Biol.* **1994**, *6*, 180–190.
(66) Schwartz, T. W. Locating ligand-binding sites in 7TM receptors by protein engineering. *Curr. Opin. Biotechnol.* **1994**, *5*, 434–444.
(67) van Rhee, A. M.; Jacobson, K. A. Molecular architecture of G protein-coupled receptors. *Drug Dev. Res.* **1996**, *37*, 1–38.
(68) Xu, W.; Li, J.; Chen, C.; Huang, P.; Weinstein, H.; Javitch, J. A.; Shi, L.; de Riel, J. K.; Liu-Chen, L.-Y. Comparison of the amino acid residues in the sixth transmembrane domains accessible in the binding-site crevices of mu, delta, and kappa opioid receptors. *Biochemistry* **2001**, *40*, 8018–8029.
(69) Shi, L.; Simpson, M. M.; Ballesteros, J. A.; Javitch, J. A. The first transmembrane segment of the dopamine D2 receptor: Accessibility in the binding site crevice and position in the transmembrane bundle. *Biochemistry* **2001**, *40*, 12339–12348.
(70) Perlman, J. H.; Colson, A. O.; Wang, W.; Bence, K.; Osman, R.; Gershengorn, M. C. Interactions between conserved residues in transmembrane helices 1, 2, and 7 of the thyrotropin-releasing hormone receptor. *J. Biol. Chem.* **1997**, *272*, 11937–11942.
(71) Sealfon, S. C.; Chi, L.; Eversole, B. J.; Rodic, V.; Zhang, D.; Ballesteros, J. A.; Weinstein, H. Related contribution of specific helix 2 and 7 residues to conformational activation of the serotonin 5-HT2a receptor. *J. Biol. Chem.* **1995**, *270*, 16683–16688.
(72) Zhou, W.; Flanagan, C.; Ballesteros, J.; Konvicka, K.; Davidson, J. S.; Weinstein, H.; Millar, R. P.; Sealfon, S. C. A reciprocal mutation supports helix 2 and helix 7 proximity in the gonadotropin-releasing hormone receptor. *Mol. Pharmacol.* **1994**, *45*, 165–170.
(73) Ballesteros, J. A.; Jensen, A. D.; Liapakis, G.; Rasmussen, S. G.; Shi, L.; Gether, U.; Javitch, J. A. Activation of the beta 2-adrenergic receptor involves disruption of an ionic lock between the cytoplasmic ends of transmembrane segments 3 and 6. *J. Biol. Chem.* **2001**, *276*, 29171–29177.
(74) Visiers, I.; Ebersole, B. J.; Dracheva, S.; Ballesteros, J.; Sealfon, S. C.; Weinstein, H. Structural motifs as functional microdomains in G-protein-coupled receptors: Energetic considerations in the mechanism of activation of the serotonin 5-HT2a receptor by disruption of the ionic lock of the arginine cage. *Int. J. Quantum Chem.* **2002**, *88*, 65–75.
(75) Javitch, J. A.; Fu, D.; Liapakis, G.; Chen, J. Constitutive activation of the beta2 adrenergic receptor alters the orientation of its sixth membrane-spanning segment. *J. Biol. Chem.* **1997**, *272*, 18546–18549.
(76) Gether, U.; Lin, S.; Ghanouni, P.; Ballesteros, J.; Weinstein, H.; Kobilka, B. Agonists induce conformational changes in transmembrane domains III and VI of the beta2 adrenoceptor. *EMBO J.* **1997**, *16*, 6737–6747.
(77) McAllister, S. D.; Hurst, D. P.; Barnett-Norris, J.; Lynch, D.; Reggio, P. H.; Abood, M. E. Structural mimicry in class A G protein-coupled receptor rotamer toggle switches: the importance of the F3.36(201)/W6.48(357) interaction in cannabinoid CB1 receptor activation. *J. Biol. Chem.* **2004**, *279*, 48024–48037.
(78) Pan, X.; Ikeda, S. R.; Lewis, D. L. SR 141716A acts as an inverse agonist to increase neuronal voltage-dependent Ca^{2+} currents by reversal of tonic CB1 cannabinoid receptor activity. *Mol. Pharmacol.* **1998**, *54*, 1064–1072.
(79) Ryckaert, J. P.; Ciccotti, G.; Berendsen, H. J. C. Numerical integration of the Cartesian equations of motion for a system with constraints: Molecular dynamics of *n*-alkanes. *J. Comput. Phys.* **1977**, *23*, 327–333.
(80) Laskowski, R. A.; MacArthur, M. W.; Moss, D. S.; Thornton, J. M. PROCHECK: A program to check the stereochemical quality of protein structures. *J. Appl. Crystallogr.* **1993**, *26*, 283–291.
(81) Morris, A. L.; MacArthur, M. W.; Hutchinson, E. G.; Thornton, J. M. Stereochemical quality of protein structure coordinates. *Proteins* **1992**, *12*, 345–364.
(82) Verdonk, M. L.; Cole, J. C.; Hartshorn, M. J.; Murray, C. W.; Taylor, R. D. Improved protein-ligand docking using Gold. *Proteins: Struct., Funct., Bioinf.* **2003**, *52*, 609–623.
(83) Berendsen, H. J. C.; Postma, J. P. M.; van Gunsteren, W. F.; DiNola, A.; Haak, J. R. Molecular dynamics with coupling to an external bath. *J. Chem. Phys.* **1984**, *81*, 3684–3690.

JM070566Z